



1 **Yields and molecular composition of gas phase and secondary**
2 **organic aerosol from the photooxidation of the volatile consumer**
3 **product benzyl alcohol: formation of highly oxygenated and**
4 **hydroxy nitroaromatic compounds**

5

6 Mohammed Jaoui¹, Kenneth S. Docherty², Michael Lewandowski¹, Tadeusz E. Kleindienst¹

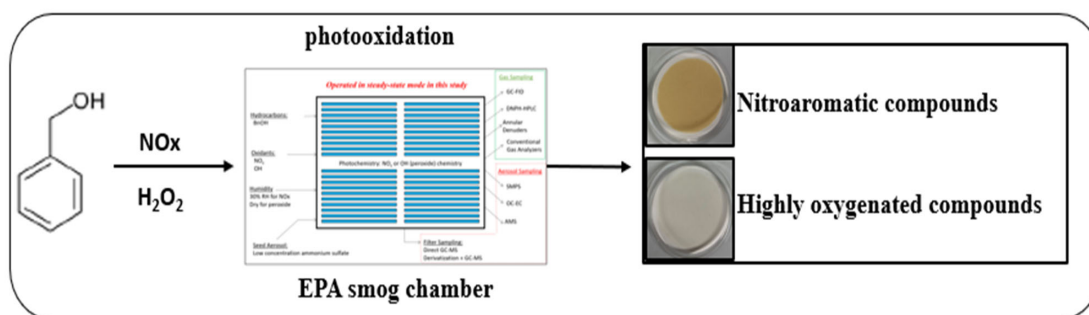
7 ¹Center for Environmental Measurement & Modeling, U.S. Environmental Protection Agency, Research Triangle Park,
8 NC, 27711, USA

9 ²Jacobs Technology, Inc., Research Triangle Park, NC, 27709, USA

10 *Correspondence:* Mohammed Jaoui (Jaoui.mohammed@epa.gov)

11

12



13

14

15

16

17

18

19

20



21 **Abstract.** Recently, volatile chemical products (VCPs) have been increasingly recognized as important precursors for
22 secondary organic aerosol (SOA) and ozone in urban areas. However, their atmospheric chemistry, physical
23 transformation, and their impact on climate, environment, and human health remain poorly understood. Here, the yields
24 and chemical composition at the molecular level of gas and particle phase products originating from the photooxidation
25 of one of these VCPs, benzyl alcohol (BnOH), are reported. The SOA was generated in the presence of seed aerosol from
26 nebulized ammonium sulfate solution in a 14.5 m³ smog chamber operated in flow mode. More than 50 organic
27 compounds containing nitrogen and/or up to seven oxygen atoms were identified by mass spectrometry. While a detailed
28 non-targeted analysis has been made, our primary focus has been to examine highly oxygenated and nitro-aromatic
29 compounds. The major components include ring-opening products with high oxygen to carbon ratio (e.g., malic acid,
30 tartaric acids, arabic acid, trihydroxy-oxo-pentanoic acids, and pentaric acid), and ring-retaining products (e.g.,
31 benzaldehyde, benzoic acid, catechol, 3-nitrobenzyl alcohol, 4-nitrocatechol, 2-hydroxy-5-nitrobenzyl alcohol, 2-
32 nitrochloroglucinol, 3,4-dihydroxy-5-nitrobenzyl alcohol). The presence of some of these products in the gas and particle
33 phases simultaneously provides evidence of their gas/particle partitioning. These oxygenated oxidation products made
34 dominant contributions to the SOA particle composition in both low and high NO_x systems. Yields, organic mass to
35 organic carbon ratio, and proposed reaction schemes for selected compounds are provided. The aerosol yield was 5.2%
36 for BnOH/H₂O₂ at SOA concentration of 52.9 μg m⁻³ and ranged between 1.7-8.1 % for BnOH/NO_x at SOA concentration
37 of 40.0-119.5 μg m⁻³.

38
39
40
41
42
43
44
45
46
47
48

Key words: Benzyl alcohol, highly oxygenated compounds, Consumer products, VCPs, Silylation, Yield, Nitroaromatic
compounds, SOA



49 1 Introduction

50 Modeling atmospheric organic aerosol (OA) using chemical transport models (CTMs) is complex, challenging, and
51 often can lead to model-measurement discrepancies (Zhao et al., 2016). Applying CTMs to urban areas reveals that
52 traditional VOCs including combustion-related processes cannot account for the observed OA mass, leaving a substantial
53 fraction unresolved (Hayes et al., 2015). Recent studies suggest that this discrepancy is due in part to unaccounted, rapidly
54 reacting SOA and ozone precursors from unknown sources (Hodzic et al., 2009; Hayes et al., 2015; McDonald et al., 2018;
55 Akherati et al. 2019; Lu et al., 2020). Volatile chemical products (VCPs), such as personal care products, cleaning agents,
56 coatings, adhesives, and pesticides have emerged as possible sources in urban areas (McDonald et al., 2018). Their
57 emissions can be larger than those from usual sources, such as motor vehicles (Coggon et al., 2021). Laboratory, modeling,
58 and field studies for VCPs have been conducted to assess their potential to affect ambient OA and ozone formation in
59 urban and suburban locations (McDonald et al., 2018; Khare et al., 2018; Stockwell et al., 2021; Seltzer et al., 2021;
60 Gkatzelis et al., 2021; Milani et al., 2021; Pennington et al., 2021; Coggon et al., 2021). The contribution of VCPs to
61 ambient OA is not fully understood and only limited modeling studies have been reported (Mohr et al., 2015; Vlachou et
62 al., 2018; Pennington et al., 2021; Qin et al., 2021; Seltzer et al., 2021). Additionally, few experimental and chamber
63 studies of VCPs have been conducted with limited characterization of aerosol products (Wu and Johnston, 2016, 2017;
64 Harrison and Well, 2012; Charan et al., 2020, 2021; Humes et al., 2022). For example, the analysis of SOA from the
65 oxidation of cyclic methyl siloxanes (Wu and Johnston, 2016, 2017; Fu et al. 2020; Alton and Browne, 2020; Charan et
66 al., 2021) and cyclic siloxanes (Janecek et al., 2019) has been conducted. Kinetic studies with limited products
67 characterization have been reported for the oxidation of benzyl alcohol (BnOH) by hydroxyl radicals (Bernard et al.,
68 2013; Wang, 2015; Harrison and Well, 2009, 2012). Recently, Humes et al. (2022) highlight the importance of oxygenated
69 aromatic VCPs emission to generate urban SOA and oxygenated products in both gas and aerosol phases. Therefore,
70 understanding the atmospheric chemistry of VCPs is important to assess their role in air quality and climate and to improve
71 SOA chemistry in CTMs thereby allowing for better estimates in health studies and source apportionment.

72 The challenges associated with evaluating VCP impacts on urban OA can be addressed by identifying atmospheric
73 VCP concentrations and SOA markers linking those VCP to ambient particulate matter (PM). Benzyl alcohol (C_7H_8O) is
74 an important ring containing VCP used as an organic intermediate and a solvent in a wide range of applications (Antonelli
75 et al. 2002). BnOH is emitted also from flowers and flowering trees (Do et al., 1969; Horvat et al., 1990; Larsen and Poll,
76 1990; Humpf and Scheier, 1991; Boatright et al., 2004; Vallat and Dorn, 2005; Orlova et al.; 2006) and found in indoor



77 air (Weschler, 2011). Gas kinetic studies of loss rates and product distributions have been conducted using flow tubes and
78 environmental chambers. Bernard et al. (2013) examined the rate and mechanisms of the OH + BnOH reaction. Similarly,
79 Harrison and Wells (2009, 2012) investigated the rate constants for the BnOH reaction with ozone, OH and NO₃ radicals.
80 Carter et al. (2005) conducted chamber experiments to assess ozone and PM formation from BnOH and related
81 compounds. Product studies from BnOH oxidation have focused mainly on gas phase (GP) products. Several carbonyl
82 products (benzaldehyde (BnAld), formaldehyde, glyoxal, butenedial, 4-oxopentanal, 3-hydroxy-2-propanaldehyde), and
83 benzyl nitrate, o-hydroxybenzyl alcohol, o-dihydroxy benzene were reported from the above studies. With respect to the
84 particle phase (PP), Charan et al. (2020) reported aerosol yields from BnOH oxidation together with a limited number of
85 SOA products. Finally, Wang (2015) conducted a theoretical study to elucidate the reaction mechanism of the oxidation
86 of BnOH with OH radicals.

87 In this study, we report a detailed non-targeted chemical analysis of GP and SOA products originated from the
88 photooxidation of BnOH in the presence and absence of oxides of nitrogen (NO_x), with the aim to better understand the
89 chemical composition at the molecular level. Gas chromatography-mass spectrometry (GC-MS) and high-performance
90 liquid chromatography were used for the identification of a range of organic compounds including oxygenated
91 nitroaromatics and related compounds bearing up to seven oxygen atoms. Nitroaromatics are pollutants of concern due to
92 their toxicity, light-absorption properties, and relatively long residence times in the environment. Highly oxygenated
93 compounds can partition into pre-existing particles or be involved in new particle formation. Also, in the present study,
94 SOA and secondary organic carbon (SOC) yields were measured with the results compared to published data. A chemical
95 mechanism is then proposed to represent and account for selected gas- and aerosol-phase products observed in this study.
96

97 **2 Experimental methods**

98 All chemicals including N, O-bis(trimethylsilyl) trifluoroacetamide (BSTFA) derivatization reagent with 1%
99 trimethylchlorosilane (TMCS) as catalyst and benzyl alcohol (99%), 2-methyl-4-nitrophenol, L-(+)-tartaric acid, D-(-)-
100 tartaric acid, and meso-tartaric acid were purchased from Aldrich Chemical Co. (Milwaukee, WI) at the highest purity
101 available and were used without further purification. In addition to standards reported in our previous studies (Jaoui et al.,
102 2004; 2018), 3-nitrobenzyl alcohol, benzoic acid, and 4-nitrocatechol were purchased from Tokyo Chemical Industry
103 (OR, USA); while pentaric acid, 2,3-dihydroxy-4-methoxy-4-oxobutanoic acid, and arabic acid were obtained from
104 Aurum Pharmatech, LLC (NJ, USA).



105

106 **2.1 Chamber description and operation**

107 All experiments were conducted in a 14.5 m³ fixed-volume chamber having TFE Teflon coated walls and maintained
108 at a positive pressure of 0.1 Torr. The chamber operation, procedures, and instrumentation have been described previously
109 (Kleindienst et al. 2006; 2009), and here just experiment-specific details are primarily included. A combination of
110 fluorescent bulbs having radiation from 300-400 nm was used to photolyze NO₂. In the absence of NO_x, the radiation
111 system was altered to include UV-313 sunlamps to adequately photolyze H₂O₂. The chamber was operated in steady-state
112 (SS or flow) mode to provide continuously stable effluent concentrations. Under these conditions, reactants and products
113 equilibrate with the chamber surfaces to minimize irreversible losses of gases and particles. The SS operation allows for
114 extended sampling periods to improve the accuracy and precision of the measurements (Shilling et al., 2008).
115 Temperature, relative humidity, and UV light intensity were measured continuously with an uncertainty of 5%. Pre-
116 experiment and post-experiment procedures (see section 2.5 below) were routinely carried out before and after each
117 experiment to minimize contamination in the chamber. The reactant generation system provided constant sources of zero
118 air, reactants, water vapor, and ammonium sulfate (AS) seed aerosol. The reactant flow of gases (e.g., NO_x) into the
119 chamber was regulated using mass flow controllers. BnOH was injected using a syringe pump, vaporized in a heated glass
120 bulb, and injected with zero air. For experiments in the absence of NO_x, a 50% aqueous solution of H₂O₂ was vaporized
121 and injected using a second syringe pump, and photolyzed to produce OH radicals. Typical chamber AS concentrations
122 were approximately 1 µg m⁻³. Each SS experiment went through an initial transient period of 18-24 h until the reactant
123 and product concentrations reached equilibrium.

124

125 **2.2 Gas-phase measurements**

126 A wide variety of instruments were used to measure the reactants and products. Nitric oxide (NO) and NO_x were
127 measured with a TECO (Franklin, MA) oxides of nitrogen analyzer with an upstream nylon filter to remove nitric acid
128 produced from OH + NO₂. The NO_x analyzer was calibrated with a NIST-traceable NO standard. Initial H₂O₂
129 concentrations were estimated by UV absorption using the ratio of the H₂O₂ to O₃ absorbances at 254 nm, as described
130 by Kleindienst et al. (2009). Experiments in the absence of NO_x were conducted dry to avoid aqueous loss of H₂O₂. BnOH
131 concentrations in the inlet and within the chamber were measured semi-continuously using an SRI Model 8610C compact



132 gas chromatograph with flame ionization detector (GC-FID; SRI Instruments, Torrance CA). The purity of the BnOH
133 was verified with GC-MS analysis.

134 Low molecular weight carbonyls and dicarbonyls were quantified by derivatization using 2,4-dinitrophenylhydrazine
135 (Smith et al., 1989). Samples were collected at 0.5 L min^{-1} for 25 min and derivatized in a 4 mL solution of acidified
136 DNPH and then heated for 40 min at 70°C . A 15-component hydrazone standard (comprising formaldehyde-,
137 acetaldehyde-, acrolein, acetone-, propionaldehyde-, crotonaldehyde-, methacrolein-, butyraldehyde-, 2-butanone-,
138 BnAld-, glyoxal-, valeraldehyde-, m-tolualdehyde-, methylglyoxal-, and hexaldehyde; AccuStandard, Inc.) at a free
139 carbonyl concentration of $30 \mu\text{g mL}^{-1}$ for each component was used for calibration. Separate dihydrazone standards of
140 glyoxal-DNPH and methylglyoxal-DNPH were also formulated. Carbonyls were separated using a Hewlett-Packard (HP)
141 1100 HPLC system having an Agilent Zorbax ODS 4.6 x 250 mm, 5- μm column maintained at 30°C eluted with binary
142 acetonitrile-water gradient. A $10 \mu\text{L}$ injection volume was used for all standards and samples. Carbonyls were quantified
143 by UV absorption with a diode array detector set to 360 nm. Control and sample processing were managed with HP
144 ChemStation software. More highly oxidized gas-phase organic species were also collected with a 60-cm, 4-channel
145 XAD4-coated annular denuder for off-line analysis (Jaoui and Kamens, 2001). Once collected, the denuders were
146 extracted and analyzed according to the methodology described in section 2.4 below.

147

148 **2.3 Aerosol-phase: bulk parameter measurements**

149 Organic carbon (OC) was measured using a semi-continuous elemental carbon-organic carbon (EC-OC) instrument
150 (Sunset Laboratories, Tigard, OR) (Offenberg et al., 2007). The pumping system draws chamber effluent through a quartz
151 filter at a rate of 8 L min^{-1} with carbon-strip denuder to remove gas-phase organics that might interfere with the
152 measurement. With a sample collection time of 0.5 h and an analysis time of 0.25 h, the duty cycle for the measurement
153 of OC was 0.75 h (Lewandowski et al., 2015). The aerosol volume, size distribution, and total number density were
154 measured using a scanning mobility particle sizer (SMPS), (Model 3071A, TSI, Inc., Shoreview, MN) and a condensation
155 particle counter (CPC) (Model 3010, TSI, Inc., Shoreview, MN). The SMPS operating conditions were as follows: sample
156 flow 0.2 L min^{-1} ; sheath flow 2 L min^{-1} ; size scan from 19 to 982 nm.

157

158 **2.4 Molecular characterization of GP and PP oxygenated organic products**



159 A non-targeted chemical analysis was conducted focusing mainly on species bearing hydroxy and carboxylic groups
160 (Jaoui et al., 2004, 2013, 2018). For each experiment, six 47-mm glass fiber (GF) filters were taken for 24 h at a flow rate
161 of 16.7 L min⁻¹. A second set of samples used an in-line 60-cm XAD-4 coated annular denuder (followed by a GF filter)
162 and analyzed for gas-phase organic products (Jaoui and Kamens, 2001). After collection, GF filters were extracted by
163 sonication with 5 mL methanol for 1 h, and denuders were extracted with 30 mL 1:1 dichloromethane/methanol mixture
164 (Jaoui and Kamens, 2001). Prior to extraction, denuders and GF filters were spiked with *cis*-ketopinic acid (KPA), *trans*-
165 *p*-menth-6-ene-2,8-diol (PMD), and d₅₀-tetracosane (TCS) as internal/recovery standards (IS/RS). Denuder extraction
166 solvents were rotary evaporated to ~1 mL and filtered using 0.45- μ m PTFE syringe filters. A 2 μ L portion of this extract
167 was analyzed by GC-MS (Jaoui and Kamens, 2001). The remaining denuder and filter extracts were evaporated to dryness
168 under a gentle stream of N₂ at room temperature using an N-Evap evaporation bath (Organomation Associates, Inc.,
169 Berlin, MA), then derivatized with BSTFA (Jaoui et al., 2004). This technique provides a sensitive method for measuring
170 low levels of highly oxidized organic compounds, including semi- and intermediate-volatile compounds in the GP and
171 PP.

172 The GC-MS analysis was conducted on an Agilent GC (7890B) coupled with a quadrupole mass spectrometer
173 (5977B). The injector, heated to 270 °C, was operated in splitless mode. Compounds were separated on a 60-m-long, 0.25-
174 mm-i.d. RTx-5MS column (Restek, Inc., Bellefonte, PA) with a 0.25- μ m film thickness. The GC oven temperature was
175 initiated at 84 °C, held for 1 min, then increased at 8 °C min⁻¹ to 200 °C, followed by a 2-min hold, then an increase at 10
176 °C min⁻¹ to 300 °C and a 15-min hold. The ion source, ion trap, and interface temperatures were 200, 200, and 300 °C,
177 respectively. Mass spectra were collected in both the methane-chemical (CI) and electron ionization (EI) modes.

178

179 **2.5 Experimental and quality control procedures**

180 Before each experiment started, the chamber was flushed with zero air for 24 h. After the reactants reached
181 equilibrium concentrations, the background was characterized using all instruments to check for artifacts including
182 background GP and PP species. Background chamber air was also characterized using off-line analysis of denuder and/or
183 filters as described above. Previous studies show that BnAld and to a lesser extent benzoic acid, benzyl benzoate and
184 dibenzyl ether present either as impurity, or as decomposition products upon BnOH exposure to air at room temperature
185 or sonication (Urakami et al., 2000; Ferri et al., 2006; Abend et al., 2004). Here we investigated the effect of chamber air,
186 sonication, and BSTFA derivatization on BnOH artifacts as described in the supplementary information (SI) in section 1.



187 A small amount of BnAld impurity was detected using the direct injection (DI) method and estimated to be <0.1% in the
188 purchased solution. When BnOH was exposed to clean air in the chamber in the absence of light, sonication, and/or
189 BSTFA derivatization, our results show additional low level of BnOH conversion to BnAld and benzoic acid using DI
190 and BSTFA methods, which is similar to the findings of Abend et al. (2004), Urakami et al. (2000), and Ferri et al. (2006).
191 Additional results and descriptions are provided in section S1 (SI).

192 Experiments were initiated by turning on the lights and allowing the irradiated chamber effluent to reach SS
193 conditions over a 24-h period which permits active sampling by the on-line instruments and the collection of denuder and
194 filter samples for subsequent off-line analysis. For organic intermediates wall losses are typically not an issue due to
195 reactions being conducted within a Teflon chamber. This potential issue is mitigated further from operating the chamber
196 in a SS mode where compound loss and re-evaporation quickly comes to equilibrium. Short lifetimes of radical
197 intermediates with other gas-phase constituents also render a negligible wall-loss. The stability of BnOH in the chamber
198 was investigated and BnOH was found to be highly stable with results given in the SI (section S1). Denuders and GF filter
199 samples were also analyzed to probe reproducibility of the analytical technique. The analysis showed consistent results.

200 Gas and particle samples from BnOH photooxidation are dominated by oxygenated species, several not having
201 authentic standards, and thus a portion of each sample was derivatized. Initially, we eliminated peaks detected in blank
202 and background samples. For compounds having standards, comparisons were made between the retention times and mass
203 spectra (CI and/or EI mode) of the chamber-derived peaks and those of the standards. For compounds not having
204 standards, individual peak identifications were associated with a product peak only if its retention time and mass spectrum
205 was consistent with the fragmentation pattern of the BSTFA-derivatized compound. All recorded spectra in this study
206 were compared with those derived from reference standards, the literature, the NIST library, and an archive of mass
207 spectra from product compounds determined in our laboratory over the past twenty years.

208

209 **3 Results and discussion**

210 The initial conditions of the experiments conducted in this study are summarized in Table 1. Three NO_x experiments
211 were carried-out with initial BnOH ranging from 0.36 – 0.72 ppm and NO from 0.096 – 0.19 ppm. One experiment without
212 NO_x was conducted with initial H₂O₂ and BnOH levels of 3.0 and 0.32 ppm, respectively. NO_x experiments were
213 conducted at ~30% RH, and the H₂O₂ experiment at < 4% RH to minimize H₂O₂ uptake onto chamber surfaces. Chamber



214 temperatures were set to 25 °C. Each experiment was conducted for up to five days for samples requiring substantial
215 masses or extended collection times and frequencies.

216 Steady state concentrations of NO, BnOH, O₃, and NO_y for the four experiments are given in Table 2. The reacted
217 BnOH and NO were calculated from the difference between the initial and steady-state concentrations. For NO_x
218 experiments, the range of reacted BnOH concentrations was 0.22 – 0.34 ppm having a reproducibility of 20–30%. Under
219 these conditions, steady state concentrations of NO_y, and O₃ were in the range of 0.08 – 0.16 and 0.011 – 0.15 ppm,
220 respectively. With NO present at steady-state, peroxy-peroxy (RO₂–RO₂) reactions were minimized. A constant aerosol
221 source was maintained for initial conditions given in Table 1. The major aerosol parameters measured (SOA, SOC, and
222 OM/OC) are given in Table 3. SOC uncertainties were taken from the reproducibility of the semi-continuous measurement
223 and typically better than 10% for a single run. For the organic mass (OM), the uncertainties are determined from the
224 reproducibility of side-by-side filter measurements which are typically better than 5%. An estimate of the systematic
225 errors due to minor changes in reactant concentrations, minor variations in chamber temperature, and similar factors bring
226 the total uncertainty to between 15-25% for these parameters (Kleindienst et al., 2009). SOA/SOC values were then
227 determined from the corrected data and given in Table 3. For experiments in the presence of NO_x, SOA/SOC values
228 ranged from 1.7-2.0. Similarly, in the absence of NO_x, the measured SOA/SOC value was 2.1.

229

230 3.1 Secondary organic aerosol and secondary organic carbon yields

231 Secondary organic aerosol yield (Y_{SOA}) and secondary organic carbon yield (Y_{SOC}) were calculated from the
232 following respective relationships $Y_{\text{SOA}} = \text{SOA}/\Delta\text{HC}$ (1); $Y_{\text{SOC}} = \text{SOC}/\Delta\text{HC}_C$ (2) where SOA is the corrected organic
233 aerosol mass concentration originated from filter measurements (6 filters) and ΔHC is the reacted BnOH concentration.
234 SOC is the organic carbon concentration found in Table 3 and ΔHC_C is the reacted BnOH carbon concentration. SOA and
235 SOC were corrected for wall loss to the chamber which had previously been determined for organic aerosol to be 0.067
236 h⁻¹ (Kleindienst et al. 2012). Uncertainties in the yield come from the experimental uncertainties in SOA and SOC
237 production and the reacted BnOH concentrations. The uncertainty in the reacted BnOH results from the reproducibility
238 of the initial and steady-state values and is estimated to range from 20 - 30% given the low volatility of BnOH and
239 challenges for introducing oxygenated species into the chamber in a consistent manner. Such challenges are also present
240 in a batch mode experiment given the difficulty to determine BnOH time profiles given its volatility and high reactivity
241 toward oxidants (Shilling et al., 2008; Kroll et al., 2007). Similar findings have been reported for sesquiterpenes oxidation



242 (Jaoui et al., 2013). As a result, aerosol yields of higher accuracy are often reported to be associated with steady state as
243 opposed to batch mode experiments (Shilling et al., 2008). Moreover, in this work we explored the possibility of BnOH
244 being taken up by ammonium sulfate (AS) seed aerosol prior to start of the irradiation or by SOA after it is initiated. This
245 test was conducted using GC-MS analysis of derivatized (BSTFA) and underivatized denuder and GF filter extracts
246 collected before and after the reaction starts (SI; Section S1). Under the experimental conditions used in this study, BnOH
247 was undetected in AS and SOA, thus limiting any participation in particle chemistry that may occur.

248 The production of aerosol, and thus the yield, were found to be highly sensitive to the precise initial conditions
249 (Tables 1, 3). Yields for the four experiments are shown in Table 3. Y_{SOA} values were determined for SOA concentrations
250 from 39.6 - 119.5 $\mu\text{g m}^{-3}$ and ranged between 3.6 and 8.1%. Similarly, Y_{SOC} was measured for SOC concentrations from
251 23.2 - 58.9 $\mu\text{gC m}^{-3}$ and found to range between 2.7 and 5.1%. In the absence of NO_x , SOA and SOC yields were 5.2
252 and 3.1 % measured for SOA and SOC concentrations of 52.9 $\mu\text{g m}^{-3}$ and 24.8 $\mu\text{gC m}^{-3}$, respectively. For the two systems
253 at similar SOA concentrations ER890 and ER892, the SOA yield was higher for the experiment with NO_x . This may
254 result from the reaction of BnOH with NO_x which tends to produce high levels of BnAld (Table 4), which may undergo
255 secondary reactions leading to additional SOA formation (see section 3.3). As expected, the data in Table 3 indicate that
256 Y_{SOA} and Y_{SOC} are lower at the lower SOA and SOC concentrations, respectively.

257 These SOA and SOC yields can be compared with other studies. Recently, Charan et al. (2020) reported SOA yields
258 for the photooxidation of BnOH in the presence of NO_x with the initial OH coming from the photolysis of H_2O_2 . Their
259 chamber was operated in a batch mode and SOA yields approaching unity were reported. By contrast, three additional
260 studies reported much lower SOA yields of 0.09, 0.3, and 0.41 from McDonald et al. (2018), Carter et al. (2005), and Li
261 et al. (2018), respectively. The yield reported by McDonald et al. (2018) was based on a multi-generation oxidation model;
262 that of Carter et al. (2005) was estimated as described in the original report, and that of Li et al. (2018) was based on
263 measurements in the presence of NO_x and a surrogate urban hydrocarbon. The results of our study are much closer in
264 value to McDonald et al. (2018). The study by Charan et al. (2020) suggests that conditions can be found where BnOH
265 SOA yields are substantially greater than that found in this study and those previously reported. The major differences
266 between the Charan et al. study and the present work were the chamber-mode operation, the seed aerosol type and levels,
267 and the mix of oxidants used. While it can be difficult to compare the yields from the two studies some comments can be
268 made. (1) As noted, the Charan et al. yields result from conventional batch mode irradiations of BnOH, H_2O_2 and NO_x .
269 (2) SOA levels were measured using an SMPS which measures aerosol volume which is then converted to aerosol mass



270 using a density of $1.4 \mu\text{g nL}^{-1}$. (3) Perhaps the biggest difference between the two studies is the use of an extremely high
271 initial seed aerosol mass, approximately two orders of magnitude higher than in this study. Thus, it is possible that an
272 adsorption mechanism played a part in contributing to the measured yields. (4) Finally, the use of high initial H_2O_2
273 concentrations relative to BnOH make it possible that H_2O_2 effectively competed with BnOH for OH via the reaction of
274 $\text{OH} + \text{H}_2\text{O}_2 \rightarrow \text{HO}_2 + \text{H}_2\text{O}$ thus generating a system rich in HO_2 . Thus, aging process may be more prominent than in our
275 study. The uncertainties associated with SOA and reacted BnOH measurements and wall loss correction are unlikely to
276 account for the differences in the two studies. However, SOA yields have been reported to increase considerably as a
277 function of initial seed aerosol (Zhang et al. 2014), as well as to increase with the OH radical exposure (Wang et al.,
278 2018). Qualitatively these two factors might bring the present SOA yields into reasonable agreement with Charan et al.
279 (2020), when data were extrapolated to similar seed aerosol and OH exposures. And as previously noted, in the low initial
280 seed aerosol used in our study no benzyl alcohol was detected in the seed aerosol or deposited on SOA. As further
281 plausibility for the results from the present study, Humes et al. (2022) recently reported yields from 0.12 - 0.18 for two
282 oxygenated aromatic species (1-phenoxy-2-propanol, and phenoxy-ethanol), compounds having similar structures to
283 BnOH.

284

285 **3.2 Reaction products identification**

286 Three methods were used in this study to identify oxygenated reaction products at the molecular level: (1) DNPH as
287 derivatizing agent for small carbonyls (Smith et al. 1989); (2) BSTFA as derivatizing agent for hydroxyl and carboxylic
288 compounds for GP and PP (Jaoui et al., 2004); and (3) direct injection (DI) method providing the capability for analysing
289 slightly polar to non-polar compounds without the use of derivatization (Jaoui and Kamens, 2001). For the BSTFA and
290 DI methods, the analysis of laboratory generated GP and PP products from BnOH oxidation shows a series of organic
291 compounds containing nitro, ketone, carboxylic acid, and/or alcoholic functional groups. Many of these compounds do
292 not have authentic standards and their identifications were based on the interpretation of the mass spectra of the derivatized
293 and/or underivatized compound (Jaoui and Kamens 2001; Jaoui et al., 2004, 2005). The identification should be regarded
294 as tentative except for compounds that have authentic standards. For the BSTFA method, the recognition of characteristic
295 ions was used to guide the analysis of mass spectra of the derivatives obtained in both electron ionization (EI) and chemical
296 ionization (CI) using methane as reagent gas. BSTFA reacts with $-\text{COOH}$ and $-\text{OH}$ groups to form BSTFA derivatives.
297 Characteristic ions are m/z 73, 75, 147, and 149. Adduct ions in CI from the derivatives include m/z $\text{M}^+ + 73$, $\text{M}^+ + 41$,



298 $M^+ + 29$, and $M^+ + 1$; fragment ions include m/z $M^+ - 15$, $M^+ - 73$, $M^+ - 89$, $M^+ - 117$, $M^+ - 105$, $M^+ - 133$, and/or
299 $M^+ - 207$. The approach used for the identification is as follows: peaks detected in blank and background chamber samples
300 were eliminated first. A peak was associated with a reaction product only if its corresponding mass spectrum was
301 consistent with the fragmentation pattern of the BSTFA derivatization reagent. All recorded spectra were compared with
302 spectra derived from various reference compounds, authentic standard, NIST library, the PubChem website
303 (pubchem.ncbi.nlm.nih.gov), and/or by MS assignment. While the off-line technique is an integrated technique that
304 requires long sampling times, it does provide a sensitive method for products identification at the molecular level as well
305 as measuring low concentrations of highly oxidized organic compounds, and semivolatile compounds in the GP. Thus,
306 products found by this collection technique could be informative for possible precursors for the types of compounds that
307 may form in the PP. In the following discussion, data are first presented to support tentative identifications of oxidation
308 products in the GP and PP.

309 **Gas phase products.** GP measurements were made of major carbonyl products formed during the photooxidation of
310 BnOH including formaldehyde, acetaldehyde, acetone, methacrolein, 2-butanone, BnAld, glyoxal, and methylglyoxal.
311 Steady-state concentrations are given in Table 4. Under the conditions shown in Tables 1 and 2, high concentrations were
312 observed for BnAld and glyoxal, and to a lesser extent formaldehyde in experiments with NO_x, and high concentrations
313 of formaldehyde, acetaldehyde, and to a lesser extent BnAld and glyoxal in the experiment without NO_x. BnAld level
314 was a factor of ~5 higher in NO_x experiments compared to H₂O₂ experiments, and formaldehyde a factor of ~36 lower.
315 Glyoxal and methylglyoxal concentrations largely were similar in both NO_x and H₂O₂ experiments. The formation of
316 BnAld, glyoxal, and formaldehyde as major products (Table 4) have already been reported from the oxidation of BnOH
317 with yields of 25 (± 5), 20 (± 2), and 3.0% (± 0.2), respectively (Bernard et al., 2013; Harrison and Wells, 2012).

318 GP samples were also collected on five-channel annular denuders. Each denuder sample was extracted and analyzed
319 directly with GC-MS without derivatization. The remaining extract was silylated, and GC-MS analyzed qualitatively.
320 Typical total ion chromatograms (TIC) of GP products detected and identified in this study are shown in Figure 1. Figure
321 1 shows portions of three TIC in +EI of GP samples taken from experiments ER889 at steady state (underivatized: Figure
322 1a), ER892 (underivatized: Figure 1b), and ER889 (silylated derivatives: Figure 1c). Peaks assigned in Figure 1 were
323 identified either by comparison with an authentic standard or by MS assignment. For clarity, only the main products are
324 shown, although several peaks could not be structurally identified. SOA generated from BnOH photooxidation is



325 dominated by oxygenated ring-opening products (see below). However, ring-retaining products were among the main
326 products observed in the GP including semivolatile organic compounds (SVOCs) (Figure 1c). Chromatograms associated
327 with the underivatized samples (Figure 1a, b) were used mainly to identify BnOH and BnAld in the system, although
328 several additional peaks absent in the background chromatogram were observed. At steady state, BnOH was not reacted
329 completely as it was detected in both systems only in the GP using both DI and BSTFA methods (Figure 1). BnAld was
330 detected in both systems in the gas and particle phases, although it was not present with BSTFA method because of the
331 absence of OH or COOH groups. Figure S3 shows EI mass spectra of BnAld identified using authentic standard, and
332 those associated with three peaks eluting at 11.3, 12.0, and 12.8 min. Although no structural information could be
333 associated with these three peaks, molecular weights of 152, 152, 138 Da (all derivatized and underivatized masses are
334 Dalton (Da) but are not designated as such hereafter), were tentatively obtained.

335 Select GP products containing OH groups identified in the present study are summarized in Table 5. Table 5 contains
336 proposed structures, molecular weights of the silylated derivatives (MW_{BSTFA}) and underivatized compounds (MW),
337 formula, and the 5 most intense ions associated with BSTFA derivatives in EI mode. Table 5 shows if GP products are
338 detected also in the PP. Figure S4 shows EI mass spectra associated with selected peaks observed in Figure 1c, including
339 BnOH-1TMS, benzoic acid-1TMS, catechol-2TMS, and 2-hydroxybenzyl alcohol-2TMS. 2-Hydroxybenzyl alcohol-
340 2TMS (2OHBnOH) peak eluted at 21.4 min was one of the largest peaks detected in the chromatogram in Figure 3c. The
341 2OHBnOH-2TMS EI mass spectrum (Figure S4, bottom) shows strong characteristic fragments ions at m/z 73, 179 (M^+
342 - 89), 253 (M^+ - 15), 268 (M^+), and its corresponding CI mass spectrum shows ions at m/z 253 (M^+ - 15), 179 (M^+ - 89)
343 and weak adducts at $M^+ + 1$, $M^+ + 29$, and $M^+ + 41$ that are consistent with the presence of two (-OH) groups, indicating
344 a BSTFA derivatized molecular weight of 268 Da. Bernard et al (2013) have identified 2OHBnOH and catechol in the
345 GP of the reaction of BnOH and OH radicals. In our study, catechol was observed only in the H_2O_2 system in the PP.
346 Additional peaks were observed, which their mass spectra are consistent with products bearing OH and/or COOH groups,
347 however, their structural identification could not be obtained due to lack of authentic standards and the complexity of the
348 interpretation of their mass spectra. BnAld was reported to undergo secondary reactions (Sankar et al., 2014) and may
349 play an important role as precursor for some oxygenated species observed in this study.

350 **Particle phase products.** One of the advantages of conducting experiments in SS mode is collecting sufficient gas and
351 aerosol masses on denuders and filters for qualitative and quantitative offline analysis. In this study, aerosol collected on



352 GF filters were solvent extracted, with the resulting extracts subjected to BSTFA derivatization followed by GC-MS
353 analysis. SOA generated from both NO_x and H₂O₂ systems was dominated by oxygenated organic compounds, for which
354 mass spectra for more than 50 species have been recorded. These species may have undergone several generations of
355 atmospheric oxidation. Several individual large peaks have been detected in addition to a significant number of small
356 peaks as shown in Figure 2. Figure 2 shows portions between 9 and 28 min of the TIC chromatograms of the silylated
357 derivatives of the aerosol extracts associated with BnOH/NO_x (top) and BnOH/H₂O₂ (bottom). The portion after 28 min
358 is discussed in the next section. The chromatograms in Figure 2 can be directly compared because the chamber air sampled
359 and the amount of extract analyzed for each system were the same. This evaluation revealed that more than 70% of peaks
360 eluted from each system are identical, suggesting similar chemistry is involved in BnOH reaction products formed in the
361 presence and absence of NO_x. In addition, a series of peaks dominated by fragments with odd *m/z* were observed only in
362 BnOH/NO_x and their mass spectra were associated with nitrogen containing compounds as discussed in the NACs section
363 below. This suggests that the composition of a portion of SOA produced in the presence of NO_x is different than that
364 formed in the absence of NO_x, which can be clearly illustrated by the filters and extracts color shown in Figure 2 (bottom).
365 Consistent with the presence of nitroaromatics, filter F2 and methanol extract (E2) has lost most of the color seen in F1
366 and E1. The presence of NO_x in the system produced material (filter F1) of a deep brown color. Most species structurally
367 identified in this study have not been reported in the literature, and mass spectra associated with several peaks are provided
368 either in the main manuscript or in the SI. Additional reaction products (e.g., oligomers, organonitrates) might have been
369 present in the SOA but could not be detected based on the analytical techniques used in this study. Note that formulae, in
370 particular chemical structure, could not be obtained for several peaks recorded in this study due to challenges interpreting
371 their mass spectra. A set of compounds identified and detected before 28 min in the present study are summarized in
372 Table 5.

373 Ring retaining products (e.g., 2-hydroxy benzyl alcohol, benzoic acid, 4-hydroxy benzoic acid, and catechol) were
374 detected in the PP in both systems, while catechol was detected only in the absence of NO_x. As noted above, some ring-
375 retaining products were detected also in the GP as shown in Table 5. Salicylaldehyde and 3-hydroxybenzaldehyde were
376 present only in the GP. These two hydroxy-aldehydes may undergo additional secondary reactions leading to some ring-
377 opening products observed in this study. Representative EI mass spectra of the TMS-derivatives associated with four
378 compounds are shown in figure 3 including benzoic acid, benzene-1,2-diol (catechol), 4-hydroxybenzoic acid, and 2-
379 hydroxybenzyl alcohol. Additional EI and CI mass spectra are shown in figures S4 and S5 in the SI. The EI mass spectrum



380 of the BSTFA derivative of 2-hydroxybenzyl alcohol displayed in figure 3 shows abundant fragment ions at m/z 73, 147,
381 267 (M^+), 253 ($M^+ - 15$), and 179 ($M^+ - 89$), and weak ions at m/z 91, 223 and 163. The corresponding CI mass spectrum
382 displayed in figure S4d shows abundant fragment ions at m/z 268 (M^+), 253 ($M^+ - 15$), and 179 ($M^+ - 89$) and adduct
383 ions at m/z 293 ($M^+ + 29$) and 309 ($M^+ + 41$). This fragmentation pattern is consistent with the presence of a compound
384 with two hydroxyl groups and a benzene ring (m/z 91) having molecular weight 268 for the BSTFA derivative, and MW
385 124 for its underivatized form. Similarly, the BSTFA EI mass spectrum of 4-hydroxybenzoic acid (Figure 3c) shows
386 characteristic fragment ions at m/z 73, 193 ($M^+ - 89$), 223 ($M^+ - 60$), 267 ($M^+ - 15$) and 282 (M^+), and its CI mass
387 spectrum fragment ions at m/z 73, 193, 67 and adducts at 283, and 311. Again, these fragments and adducts are consistent
388 with the presence of two (-OH) groups and a molecular weight of the derivatized compound of 282 and 138 for the
389 underivatized compound. The presence of a peak at m/z 153 ($M^+ - 117$) is consistent with a compound bearing an organic
390 acid group. The EI mass spectra recorded in this study for 2-hydroxybenzyl alcohol and 4-hydroxybenzoic acid are
391 identical to the reference NIST spectrum (webook.nist.gov). Figure S5 shows EI mass spectra associated with four peaks
392 eluted at 12.86, 15.58, 16.24, and 19.78 min consistent with the fragmentation pattern of BSTFA derivatives, although
393 their structures could not be obtained.

394 **Highly oxygenated compounds (HOCs).** Recent studies show that highly oxygenated compounds (e.g., HOMs) play an
395 important role in understanding SOA formation (Berndt et al. 2016, Jaoui et al., 2019; 2021 and references therein, Piletic
396 and Kleindienst, 2022). These compounds may result from several generations of atmospheric oxidation. In this study,
397 several ring-opening products eluted late in the chromatograms (RT > 25 min), with a relatively high O:C ratio of > 1.3
398 likely contributes to their condensation in the PP, were detected. Three groups of these oxidation products were detected
399 in the PP in both systems. Figure 4 shows the portion between 25 and 34 min of selected GC-MS extracted-ion
400 chromatograms where these groups (color coded) elute and uses the selected ions m/z 423, 437, and 525 (merged in one
401 chromatogram) to best illustrate them: (a) BnOH/NO_x; (b) BnOH/H₂O₂; (c) chamber background. Groups 1, 2, and 3
402 consist of three (green), eight (blue) and four (red) peaks, respectively, and are completely absent from the background
403 chromatogram (figure 4c). Results from a comprehensive interpretation of EI and CI mass spectra associated with peaks
404 shown in figure 4 enabled the identification of several isomers associated with each group. Figure 5 displays three EI
405 mass spectra associated with each group main peak, along with proposed structure and chemical formulae. Table 6 gives
406 the major highly oxygenated compounds identified in this research, including the main peaks from each of these groups,
407 in the order of their underivatized molecular weight. Table 6 gives the chemical formulas, O:C mass ratio, the five most



408 abundant ions associated with each TMS derivative in methane-CI and EI modes, the molecular weights of the
409 underivatized (MW) and TMS-derivatized compounds (MW_{BSTFA}), and the proposed chemical structures of the
410 compounds.

411 Group 1 consists of *meso*-tartaric acid (*mTA*) (Rt 26.04 min), and *L-/D*-tartaric acids (*ITA/dTA*) (Rt 27.66 min)
412 identified based on authentic standards. The mass spectra of BSTFA derivatives of *ITA* and *dTA* standards (Figure S6,
413 SI) are very similar (eluting at the same time) and are only slightly different from the *mTA* (Figure S6: SI); however,
414 *ITA/dTA* and *mTA* elute at two different retention times (Figure 4, S6). The peak associated with *mTA*, and *ITA/dTA* are
415 among the largest peak observed in this portion of the chromatograms. Note, *ITA* isomer is the most abundant tartaric
416 acid present in nature (DeBolt et al., 2006). The fragments and adducts observed for the peak eluting at 25.19 min are
417 similar to those of *mTA* and *d-/ITA* and are consistent with the presence of four OH groups, a MW of 452 for the
418 derivatized compound and 164 for the underivatized compound, and a $C_4H_6O_6$ chemical formula. Tartaric acid has been
419 reported in ambient aerosol (Rohrl and Lammel, 2002; Gowda et al., 2016) and in chamber 1,3-butadiene SOA (Jaoui et
420 al., 2014). Recent studies suggest that tartaric acid and other hydroxy carboxylic acids undergo heterogeneous OH reaction
421 in aqueous solution, with the presence and position of OH group(s) playing an important role in fragmentation and
422 functionalization of organic aerosol (Cheng et al., 2016).

423 Group 2 consists of eight peaks (figure 4: blue) eluting between 28.5 and 31.5 min. The EI and CI mass spectra
424 associated with each peak display similar fragment and adduct ions across the range of 50 to 600 Da. The interpretation
425 of these mass spectra allows us to infer the molecular weight (MW) of the underivatized compounds as 164 and MW_{BSTFA}
426 of 452 for the TMS derivatives. The BSTFA CI mass spectrum of the peak eluted at 29.48 (largest peak) shows
427 characteristic fragment ions at m/z 73, 437 [$M^+ - 15$], 363 [$M^+ - 89$], and 305 [$M^+ - 105$], and an adduct at 453 [$M^+ + 1$],
428 481 [$M^+ + 29$], and 493 [$M^+ + 41$]. These fragments and adducts are consistent with the presence of four OH groups and
429 an MW of 452 for the derivatized compound and 164 for the underivatized compound. The presence of peaks at m/z 347
430 [$M^+ - 105$], and 335 ($M^+ - 117$) are consistent with a compound bearing alcoholic and carboxylic OH groups
431 simultaneously. This mass spectrum is similar to the one from methyltartaric acid reported previously from isoprene
432 oxidation by our group (Jaoui et al., 2019). The silylated methyltartaric acid mass spectrum (Jaoui et al., 2019) and mass
433 spectra associated with group 2 are only slightly different, however, they elute at different retention times. The peaks have
434 been tentatively identified as isomers of trihydroxy-oxo-pentanoic acid, with the structure of 4-oxo-D-arabonic acid
435 isomer shown in Table 6.



436 Group 3 consists of four peaks eluting between 32.5 and 34 min (figure 4: red). The EI and CI mass spectra associated
437 with each peak display similar fragment and adduct ions across the range of 50 to 600 Da. As a descriptive example, an
438 EI mass spectrum is shown in Figure 5 for peak eluted at 33.1 min. A comprehensive interpretation of EI and CI mass
439 spectra associated with group 3 peaks (Figures 4, 5), allows us to infer the molecular weight (MW) of the underivatized
440 compounds as 180, and MW_{BSTFA} of 540 for the TMS derivatives, with a chemical formulae $C_5H_8O_7$. The compounds
441 corresponding to these four peaks were identified as isomers of C_5 -trihydroxydicarboxylic acids. This identification is
442 tentative due to the absence of authentic standards, except for peak eluting at 33.47, which was identified as pentaric acid
443 (Table 6) based on authentic standard. The spectra of BSTFA derivatives of the remaining three red peaks are only slightly
444 different from the pentaric acid spectrum (Figure 6); however, they elute at different retention times. The EI mass spectra
445 are also similar to those reported in the literature for a set of C_5 -aldaric acids-TMS derivatives including xylic, arabinaric
446 and ribaric acids (Hinton et al., 2008; <https://pubchem.ncbi.nlm.nih.gov>). Figure 6 shows the structure of pentaric acid
447 and its four isomers (a), the spectra associated with BSTFA derivative of pentaric acid observed in BnOH SOA (b: EI
448 mode), (c: CI- CH_4 mode), and standard (d: EI mode). Figure 6 also shows the structure of the main fragments observed
449 in BSTFA derivative of pentaric acid in EI mode including m/z at 540, 525, 407, 292, 147, and 73 Da. Pentaric acid and
450 its isomers (aldaric acids) are reported to be formed from the oxidation of aldopentose (Hinton, 2008; Derrien et al., 2018),
451 but no evidence has been provided for its presence in SOA samples. In the present study, we successfully identified aldaric
452 acids from the oxidation of BnOH in SOA samples.

453

454 **Nitroaromatic compounds (NACs).** NACs of secondary origin are a possible contributor to urban OA and not only
455 adversely affect human health and the environment but impact the aerosol optical properties and the atmospheric radiation
456 balance. By understanding the sources of NACs in ambient particles and their chemical identities, we can evaluate their
457 impact on the climate, environment, and human health. Recently, the analytical capabilities associated with BSTFA
458 derivatization have been extended to NACs bearing hydroxyl and carboxylic acid groups (Jaoui et al., 2018). Mass spectra
459 of most silylated NACs, especially methane-Cl, are highly specific, reproducible, and produce characteristic fragments
460 useful in determining structural information and molecular weight, when authentic standards are not available (Jaoui et
461 al., 2018). In this study, a detailed analysis of mass spectra associated with peaks in chromatograms Figure 1c (GP) and
462 Figure 2 top (PP) reveals the presence of several peaks presenting similar fragmentation patterns as those reported by
463 Jaoui et al. (2018) for species bearing hydroxyl, carboxylic, nitro groups, and benzene ring. Figure 7 shows the portion



464 between 23 and 42 min of two +EI extracted ion chromatograms for the BSTFA derivatives at m/z 210, 165 (IS), 299 (IS),
465 300, 298, 372, 388 (merged in one chromatogram) associated with BnOH/NO_x (top) and BnOH/H₂O₂ (bottom). The EI
466 and/or CI mass spectra of selected nitroaromatic standards can be found in Jaoui et al. (2018), and additional representative
467 subset of the derivatives are displayed in Figures S7 (SI). For clarity, figure 7 inset shows an expanded portion of the top
468 chromatogram between 26.7 – 28 min. Table 7 contains proposed identification of NACs detected in this study, along
469 with molecular weights, formulae, main 5 intense ions associated with CI and EI mass spectra of the derivatives, proposed
470 structure, and the GP to PP peak area ratio.

471 NACs with the highest confidence assignment are those identified by comparing their retention times, EI, and CI
472 mass spectra with those of reference standards, and NACs with low levels of confidence are those (1) that have been
473 identified previously in ambient PM or in smog chamber studies, (2) their EI mass spectra exist in the literature, or (3)
474 their molecular weights and numbers of OH, COOH, and NO₂ groups are simply consistent with the CI and EI mass
475 spectrum (Jaoui et al., 2018). A total of fourteen peaks associated with NACs were detected in this study. 3-Nitrobenzyl
476 alcohol, 4-nitrocatechol, 2-hydroxy-5-nitro benzyl alcohol, and 2-nitrophloroglucinol were identified based on authentic
477 standards. Three peaks eluted at 33.76, 34.70, and 34.76 having similar mass spectra as 2-nitrophloroglucinol (main peak)
478 eluted at 35.62 min were detected. They were tentatively associated with homologous series of 2-nitrophloroglucinol
479 including 3-nitrobenzene-1,2,4-triol, 5-nitropyrogallol, and 4-nitro-1,2,3-benzenetriol (not shown in Table 7). Similarly,
480 three additional peaks having similar mass spectra as 2-hydroxy-5-nitrobenzyl alcohol were observed and were tentatively
481 associated with homologous series of 2-hydroxy-5-nitrobenzyl alcohol including 4-hydroxy-2-nitrobenzyl alcohol. The
482 EIC in figure 7 (top) includes a series of four peaks observed only in the PP eluting at 35.94, 36.60, 38.18 min, whose
483 mass spectra were consistent with the presence of molecular weight 185 and 401 for the underivatized and derivatized
484 compounds, respectively. Based on similarity of their mass spectra, they were tentatively identified as structural
485 homologue of 3,4-dihydroxy-5-nitrobenzyl alcohol (Table 7) with C₇H₇NO₅ formulae. As can be seen in figure 7 (bottom),
486 NACs peaks were not detected in BnOH/H₂O₂ SOA extract, consistent with the formation of NACs in the presence of
487 NO_x. All NACs were detected in both GPs and PP (Table 7), except 2-nitrophloroglucinol and 3,4-dihydroxy-5-
488 nitrobenzyl alcohol and their isomers were observed only in the PP consistent with their low volatility. This result suggests
489 that NACs may be formed in the GP, and partition to the PP for those with low volatility, although PP reactions may
490 occur as suggested by Charan et al. (2020) who analyzed only PP. 4-Nitrocatechol and 2-nitrophloroglucinol were among
491 the largest NAC peaks observed in our study (Figure 7). All three experiments conducted in this study were analyzed for



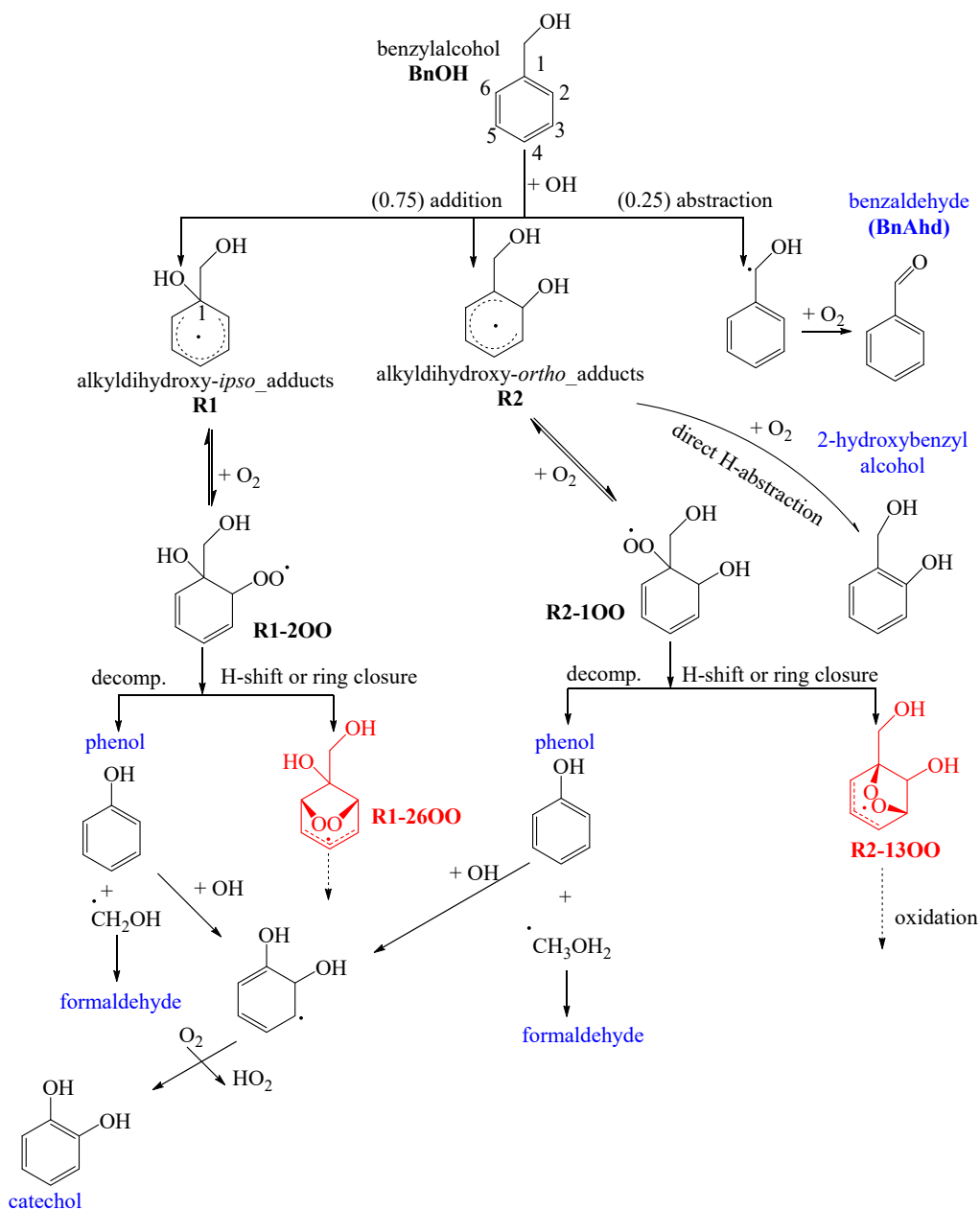
492 NACs to probe reproducibility of the BSTFA method and showed consistent results. 2-Nitrophenol, 4-
493 nitrocatechol and other NACs has been reported in PM collected in Pico Mountain Observatory, Pico Island in the Azores
494 archipelago by Ikemori et al., (2019). A series of NACs have been reported recently by Charan et al. (2020) in BnOH
495 SOA using off-line UPLC/ESIQ-ToFMS (ultra-high-performance liquid chromatography electrospray ionization
496 quadruple time of flight mass spectrometry), and the structure assigned to formulas obtained from MassLynk software
497 was based on expected oxidation products and MS/MS analysis. These observations support the identification of NACs
498 reported in this study. 4-Nitrophenol was reported in the GP by Bernard et al., (2013) at low yield and by Charan et al.
499 2020 in SOA from the OH radical oxidation of BnOH but was not detected either in the GP or the PP in this study.

500

501 3.3. Mechanism of product formation

502 Based on known GP reactions for aromatic compounds, a schematic representation for the reaction of BnOH with
503 OH is presented in schemes 1-3. It is developed to understand the chemistry leading to the main GP and PP products
504 identified experimentally in this study including HOCs and NACs. These schemes incorporate the latest experimental,
505 quantum and kinetic developments of the fate of peroxy/alkoxy benzoyl radicals including autooxidation (Wang, 2015;
506 Sankar et al. 2014, and Namysl et al. 2020). The lines shown in these schemes are either one step or multistep pathways.
507 Rate constants at room temperature of BnOH with OH radical, O₃, and NO₃ radical of 2.8 10⁻¹¹, 6 x 10⁻¹⁹ (upper limit),
508 and 4.0 x 10⁻¹⁵ cm³ molecule⁻¹ s⁻¹, respectively, have been reported in the literature (Harrison and Wells, 2009, 2012;
509 Bernard et al., 2013). This suggests that the day-time oxidation of BnOH will be mainly initiated by OH radicals. The
510 reaction for O₃ and NO₃ radical are not included in schemes 1-3, although they are expected to be formed as minor
511 products in our systems.

512 The reaction of BnOH with OH radicals is initiated primarily by H atom abstraction from the external CH₂ group
513 leading to BnAld, and OH addition to the aromatic *ipso* (C1) and *ortho* (C2 or C6) positions to form two alkyldihydroxy
514 adducts R1 and R2 (scheme 1). The OH addition to the *para* (C3, C5) and *meta* (C4) position was reported to be not
515 favourable based on theoretical study of Wang, (2015). Scheme 1 shows mechanistic pathways leading to the formation
516



517

518 **Scheme 1.** Initial reaction pathways proposed to produce selected products detected in this study (blue color) in the gas
519 or PP (Table 5). R1-26OO and R2-13OO intermediates undergo further reactions leading to ring-opening products as
520 shown in scheme 3.

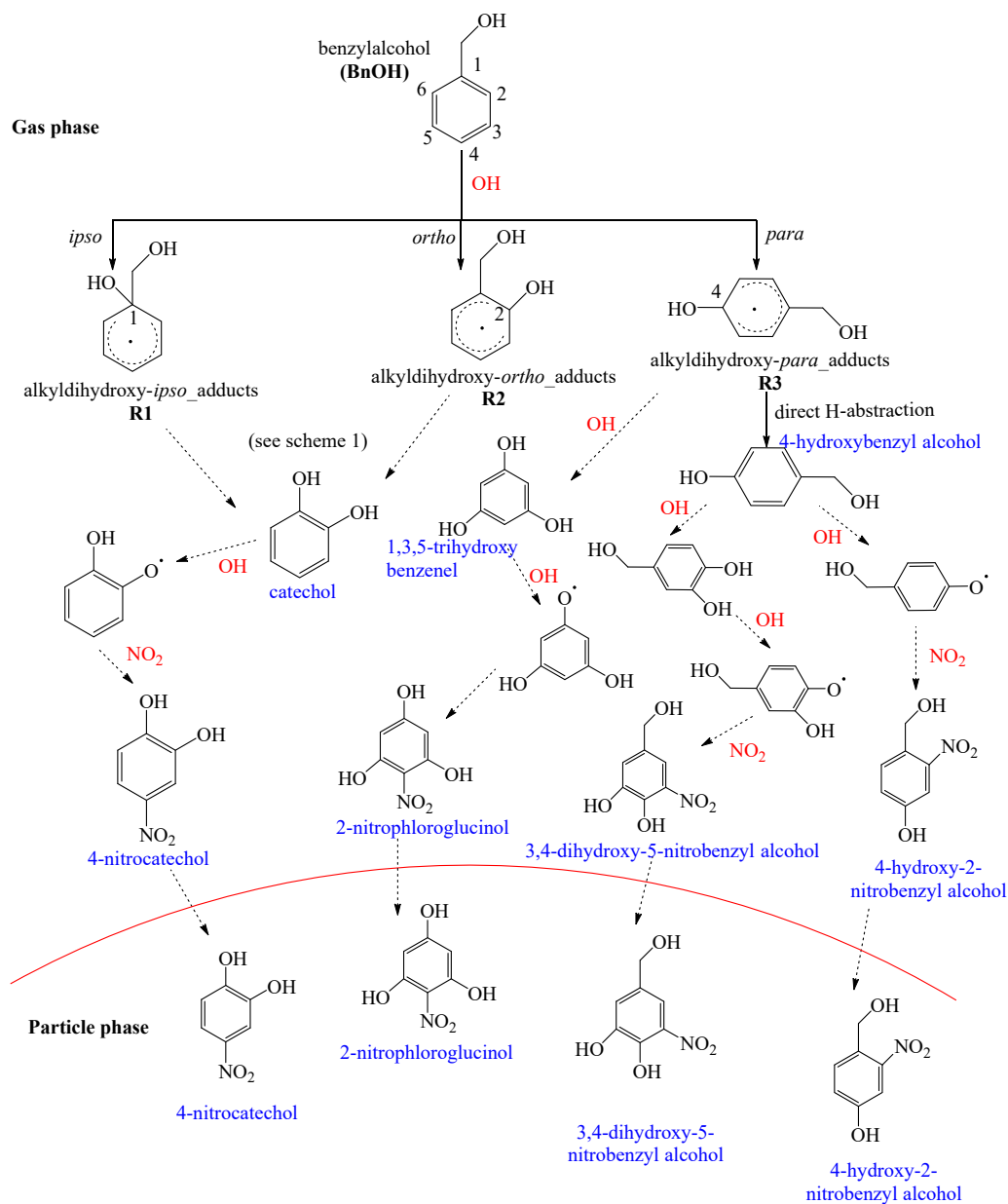
521



522 of stable products (blue) including BnAld, 4-hydroxybenzyl alcohol, 2-hydroxybenzyl alcohol, phenol, formaldehyde,
523 and catechol. The initial branching ratios shown in scheme 1 are those reported by Wang (2015), obtained by combining
524 quantum chemistry calculations and experimental work from the literature. BnAld was observed in this study in the
525 presence and absence of NO_x, and its secondary chemistry may lead in part to oxygenated compounds observed in this
526 study (Bernard et al., 2013). Due to large number of possible intermediates formed (Wang, 2015), only selected pathways
527 energetically favourable leading to some products observed in this study are considered. We refer the readers to Wang
528 (2015) paper for an in-depth theoretical analysis of mechanistic pathways leading to the formation of selected reaction
529 products. The adduct R1 reacts rapidly through addition of O₂ to the ortho (C2) to produce peroxy radicals R1-2OO, The
530 O₂ addition to para position (C4) leading to R1-4OO peroxy radicals (not shown in Scheme 1) was found to be
531 endothermic, therefore negligible (Wang, 2015). Radicals R1-2OO undergo intramolecular H-shifts or ring closures to
532 form a stable bicyclic intermediate R1-26OO (red). Similarly, R2 reacts rapidly with O₂ to form peroxy radical R2-1OO
533 intermediate, which itself undergoes intramolecular H-shifts or ring closures to form a stable bicyclic intermediate R2-
534 13OO (red). R1-26OO and R2-13OO intermediates undergo further reactions leading to ring-opening products as shown
535 in scheme 3 below. 2-Hydroxybenzyl alcohol was proposed by Wang (2015) to form through the reaction of R2 with O₂
536 involving rapid direct H-abstraction. A possible formation pathway of phenol is decomposition of the peroxy radicals R1-
537 2OO and R2-1OO through CH₂OH radical elimination (Bernard et al., 2013). CH₂OH radical reacts rapidly with O₂ to
538 produce formaldehyde. Catechol was proposed to originate from the reaction of OH radicals with phenol (Atkinson et al.,
539 1992) and with 2-hydroxybenzyl alcohol (Bernard et al., 20013).

540 NACs observed in this study (Table 7) are expected to be formed through reaction of OH radicals with BnOH in the
541 presence of NO₂. Scheme 2 briefly summarizes the main mechanistic pathways leading to BnOH NACs, which follow
542 similar chemistry as those reported for toluene, benzene, and xylenes (Jenkin et al., 2003; Vidovic et al., 2018) and
543 summarized by Wang et al., (2019). The steps shown in scheme 2 are multi-steps and the reader should consult the
544 reference papers above for more in depth information. NACs are proposed to originate from secondary reactions of
545 catechol, 1,3,5-trihydroxy benzene, and 4-hydroxybenzyl alcohol with OH radicals in the presence of NO₂ (scheme 2).
546 These intermediates are proposed to be originated from R1, R2, and R3 adducts. Additional pathways could be initiated
547 via less well understood aqueous-phase nitration (Krofljic et al., 2018). 4-Nitrocatechol is proposed to be initiated through
548 the reaction of catechol with OH radicals in the presence of NO_x (Finewax et al., 2018). 4-Hydroxy-2-nitrobenzyl alcohol
549 is proposed to be likely originated from the alkyldihydroxy-para-adduct formed from the OH addition to para position

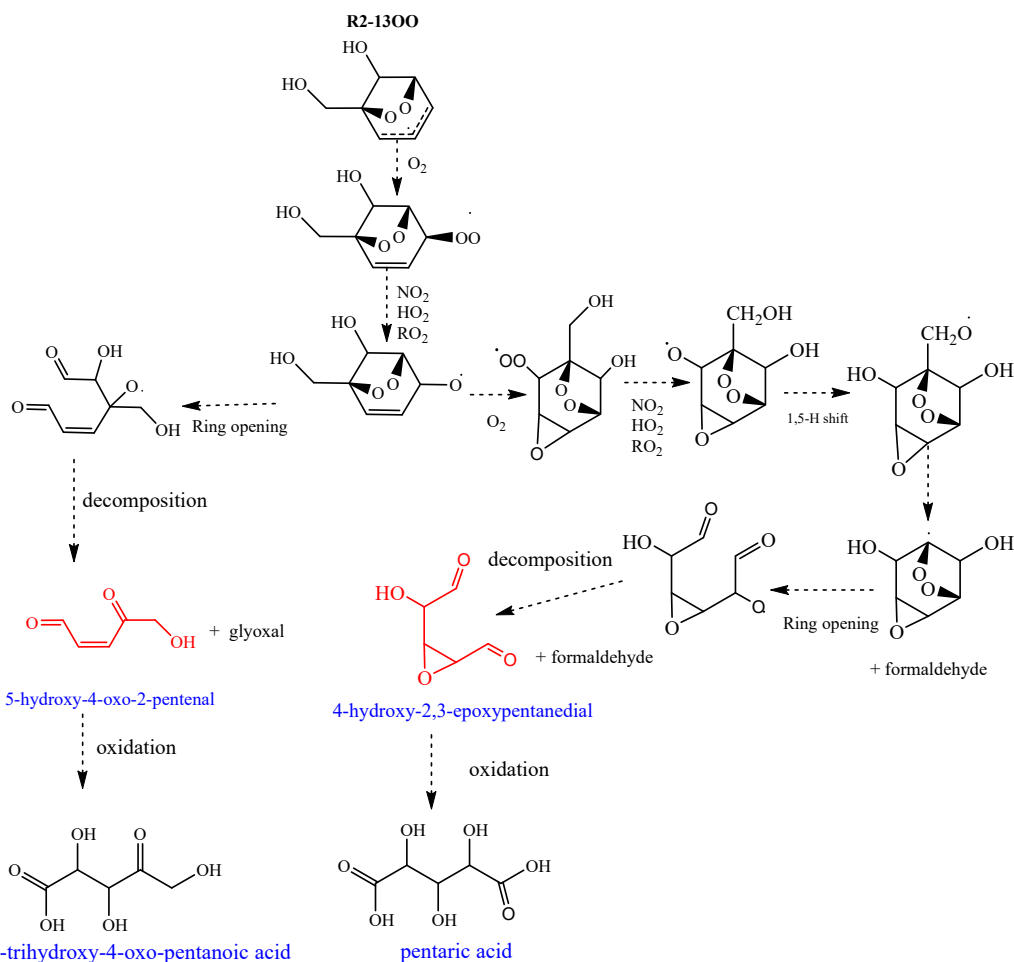
550 (scheme 2). 2-Nitrophenlorucinol and 3,4-dihydroxy-5-nitrobenzyl alcohol follow similar reactions involving R3 adduct,
 551 OH radicals, and NO₂.



552
 553 **Scheme 2.** Proposed mechanism for selected NAC species observed in this study.
 554



555 HOCs were detected in the PP from the oxidation of BnOH in both low and high NO_x systems (Table 6). Mechanistic
556 pathways based on theoretical studies leading to several HOCs (e. g. HOMs) from the atmospheric oxidation of biogenic
557 and aromatic hydrocarbons have been reported recently in the literature involving unimolecular reaction through
558 autoxidation, and peroxy and/or alkoxy radical isomerization (Wang, 2015; Jaoui et al., 2021; Piletic and Kleindienst,
559 2022). The formation of selected HOCs observed in this study is consistent with the following pathways proposed in
560 scheme 3 involving R2-1300 radical as the starting material. R1-26OO adduct undergoes similar reactions leading to
561 butenedial and 2,3-epoxy-butanedial as shown in scheme S1 (SI). Tartaric acid, 2,3,5-trihydroxy-4-oxo-pentanoic acid,
562 and pentaric acid, observed in this study for the first time, are proposed to be initiated by the oxidation of butenedial/2,3-
563 epoxy-butanedial, 5-hydroxy-4-oxo-2-pentenal, and 4-hydroxy-2,3-epoxypentandial



564 2,3,5-trihydroxy-4-oxo-pentanoic acid

pentaric acid

565 **Scheme 3.** Proposed mechanism for selected highly oxygenated compounds observed in this study.



566
567 (scheme 3). The mechanism leading to butenedial/2,3-epoxybutanal, 5-hydroxy-4-oxo-2-pentanal (scheme S1) was
568 reported by Wand (2015) from the OH oxidation of BnOH, therefore is not shown in scheme 3. Tartaric acid present in
569 the PP at high level (Figure 4), is proposed to be formed through the oxidation of butenedial and/or 2,3-epoxybutanal
570 through classical oxidation of aldehydes and alkenes to carboxylic acid (not shown in scheme 3). Similarly, 2,3,5-
571 trihydroxy-4-oxo-pentanoic acid and pentaric acid are proposed to rise from the oxidation of 5-hydroxy-4-oxo-2-pentanal,
572 and 4-hydroxy-2,3-epoxypentanedial, respectively following similar mechanistic pathways reported by Jaoui et al. (2021)
573 for the formation of methyltartaric acid from 4-hydroxy-2-methyl-but-2-enal involving peroxy and alkoxy radical
574 isomerization (not reported here). In this study, a new mechanism is proposed in scheme 3 leading to the formation of 4-
575 hydroxy-2,3-epoxypentanedial, which is the starting material for pentaric acid formation. It involves several intermediate
576 steps including unimolecular H migration (e.g., 1,5-H shift), ring opening and decomposition. Formaldehyde and glyoxal
577 observed in this study are also shown in scheme 3.

578

579 **4. Summary**

580 In the present manuscript, laboratory experiments were conducted to investigate SOA formation from the oxidation
581 of benzyl alcohol in the presence and absence of NO_x. Chamber aerosol collected under these conditions has been
582 analyzed for organic mass to organic carbon ratio, and aerosol yield. In addition, the chemical composition of the gas
583 phase and SOA was analyzed using derivative-based methods followed by gas chromatography-mass spectrometry and
584 high-performance liquid chromatography analysis of the derivative compounds. More than 50 oxygenated organic
585 compounds in the gas and particle phases were identified. While a detailed non-targeted analysis has been made, our
586 primary focus has been to examine highly oxygenated and nitroaromatic compounds. The major components include ring-
587 opening products with high oxygen to carbon ratio (e. g. malic acid, tartaric acid, arabic acid, 2,3,5-trihydroxy-4-oxo-
588 pentanoic acid, and pentaric acid) and ring-retaining products (e. g. benzaldehyde, benzoic acid, catechol, 3-nitrobenzyl
589 alcohol, 4-nitrocatechol, 2-hydroxy-5-nitrobenzyl alcohol, 2-nitrophenol, 5-(hydroxymethyl)-3-nitro-1,2-benzyl
590 diol). The presence of some of these products in the gas and particle phases simultaneously provides evidence of their
591 gas/particle partitioning. These oxygenated oxidation products made dominant contributions to the SOA particle
592 composition in both low and high NO_x systems. Yields, organic mass to organic carbon ratio, and proposed reaction
593 schemes for selected compounds are provided.



594 Finally, a set of reaction pathways are proposed that accounts for selected reaction products observed in this study
595 from BnOH photooxidation in the presence of OH radicals, including NACs and HOCs. The proposed mechanism is
596 based on (1) theoretical studies reported previously in the literature and (2) mechanisms associated with aromatics
597 oxidation (e.g., benzene, toluene, xylenes...). New pathways were proposed for the formation of newly observed highly
598 oxygenated compounds tartaric acid, 2,3,5-trihydroxy-4-oxopentanoic acid, and pentaric acid. Butenedial/2,3-epoxy-
599 butandial, 5-hydroxy-4-oxo-2-pentenal, and 4-hydroxy-2,3-epoxypentanedial were proposed as the starting intermediate
600 species leading to these highly oxygenated compounds. While theoretical studies involving unimolecular reactions were
601 developed focusing mainly on ring-containing products (Wang, 2015, Piletic and Kleindienst, 2022), similar theoretical
602 investigations focusing on linear species (Jaoui et al., 2021) as HOCs reported in this study will help strengthen the
603 pathways proposed here.

604 The results of this study potentially have atmospheric implications for areas impacted by benzyl alcohol including
605 urban and indoor areas and contribute to understanding the formation of ambient SOA from oxygenated anthropogenic
606 precursors. Nitroaromatics are pollutants of concern due to their toxicity, light-absorption properties, and relatively long
607 residence times in the environment. HOCs may partition into pre-existing particles or be involved in new particle
608 formation.

609
610
611

612 *Data Availability.* The data used in this study can be found at: <https://catalog.data.gov/dataset/epa-sciencehub>. DOI:
613 10.23719/1527893.

614

615 *Competing interests.* The authors declare no competing financial interest.

616

617 *Disclaimer.* This work has been subjected to the U.S. Environmental Protection Agency's administrative review and
618 approved for publication. The views expressed in this article are those of the authors and do not necessarily represent the
619 views or policies of the U.S. Environmental Protection Agency. Mention of trade names does not constitute endorsement
620 or recommendation of a commercial product by U.S. EPA.

621

622

623



624 **References**

625 Abend, A. M., Chung, L., Bibart, R. T., Brooks, M., and McCollum, D. G.: Concerning the stability of benzyl alcohol:
626 formation of benzaldehyde dibenzyl acetal under aerobic conditions, *J. Pharm. Biomed. Anal.*, 34, 5, 957-962,
627 doi:10.1016/j.jpba.2003.11.007, 2004.

628

629 Akherati, A., Cappa, C. D., Kleeman, M. J., Docherty, K. S., Jimenez, J. L., Griffith, S. M., Dusanter, S., Stevens, P. S.,
630 and Jathar, S. H.: Simulating secondary organic aerosol in a regional air quality model using the statistical oxidation
631 model - Part 3: Assessing the influence of semi-volatile and intermediate-volatility organic compounds and NO_x, *Atmos.*
632 *Chem. Phys.*, 19, 4561–4594, 2019.

633

634 Alton, M. W., and Browne, L. C.: Atmospheric chemistry of volatile methyl siloxanes: kinetics and products of oxidation
635 by OH radicals and Cl atoms, *Environ. Sci. Technol.*, 54, 5992–5999, 2020.

636

637 Antonelli, L., Mapelli, E., Strini, A., Cerulli, T., Leoni, R., and Stella S.: Laboratory and real scale comparative study of
638 benzyl alcohol emission from a two-component epoxy paint, *Proceedings: Indoor Air*, 584-589, 2002.

639

640 Atkinson, R., Aschmann, S. M., and Arey, J.: Reactions of OH and NO₃ Radicals with Phenol, Cresols, and 2-Nitrophenol
641 at 296 ± 2 K, *Environ. Sci. Technol.* 1992, 26, 1397-1403, 1992.

642

643 Bernard, B., Magneron, I., Eyglunent, G., Daële, V., Wallington, T. J., Hurley, M. D., and Mellouki, A.: Atmospheric
644 chemistry of benzyl alcohol: kinetics and mechanism of reaction with OH radicals, *Environ. Sci. Technol.*, 47,
645 3182–3189, 2013.

646

647 Berndt, T., Herrmann, H., Sipila, M., and Kulmala, M.: Highly oxidized second-generation products from the gas-phase
648 reaction of OH radicals with isoprene. *J. Phys. Chem. A*, 120 (51), 10150– 10159, 2016.

649

650 Boatright, J., Negre, F., Chen, X., Kish, C. M., Wood, B., Peel, G., Orlova, I., Gang, D., Rhodes, D., and Dudareva, N.:
651 Understanding in vivo benzenoid metabolism in petunia petal tissue, *Plant Physiol.*, 135, 1993–2011, 2004.



652

653 Carter, W. P. L., Malkina, I. L., Cocker III, D. R., and Song, C.: Environmental chamber studies of VOC species in
654 architectural coating and mobile source emissions, South Coast Air Quality Management District Contract No. 03468,
655 2005.

656

657 Charan, S. M., Buenconsejo, R. S., and Seinfeld, J. H.: Secondary organic aerosol yields from the oxidation of benzyl
658 alcohol, *Atmos. Chem. Phys.*, 20, 13167–13190, doi:10.5194/acp-2020-49, 2020

659

660 Charan, S. M., Huang, Y., Buenconsejo, R. S., Li, Q., Cocker III, D. R., and Seinfeld, J. H.: Secondary organic aerosol
661 formation from the oxidation of decamethylcyclopentasiloxane at atmospherically relevant OH concentrations, *Atmos.*
662 *Chem. Phys.*, 22, 917-928, doi:10.5194/acp-22-917-2022, 2021.

663

664 Cheng, C. T., Chan, M. N., and Wilson, K. R.: Importance of unimolecular HO₂ elimination in the heterogeneous OH
665 reaction of highly oxygenated tartaric acid aerosol, *J. Phys. Chem. A*, 120, 5887–5896, doi: 10.1021/acs.jpca.6b05289,
666 2016.

667

668 Coggon, M. M., Gkatzelis, G. I., McDonald, B. C., Gilman, J. B., Schwantes, R. H., Abuhassan, N., Aikin, K. C., Arendt,
669 M. F., Berkoff, T. A., Brown, S. S., Campos, T. L., Dickerson, R. R., Gronoff, G., Hurley, J. F., Isaacman-VanWertz, G.,
670 Koss, A. R., Lia, M., McKeen, S. A., Mosharyd, F., Peischl, J., Pospisilova, V., Renh, X., Wilson, A., Wu, Y., Trainer,
671 M., and Warneke, C.: Volatile chemical product emissions enhance ozone and modulate urban chemistry,
672 doi:10.1073/pnas.2026653118, *PNAS*, 118, 32, e2026653118, 2021.

673

674 DeBolt, S., Cook, D. R., and Ford, C. M.: L-Tartaric acid synthesis from vitamin C in higher plants, *PNAS*, 103 (14) 5608-
675 5613, doi: 10.1073/pnas.0510864103, 2006.

676

677 Derrien, E., Ahmar, M., Martin-Sisteron, E., Raffin, G., Queneau, Y., Marion, P., Beyerle, M., Pinel, C., and Besson, M.:
678 Oxidation of aldoses contained in softwood hemicellulose acid hydrolysates into aldaric acids under alkaline or



- 679 noncontrolled pH conditions, *Industrial & Engineering Chemistry Research*, 57 (13), 4543-4552, doi:
680 10.1021/acs.iecr.8b00239, 2018.
- 681
- 682 Do, J. Y., Salunkhe, D. K., and Olson, L. E.: Isolation, identification and comparison of the volatiles of peach fruit as
683 related to harvest maturity and artificial ripening, *J. Food Sci.*, 34, 618–621, 1969.
- 684
- 685 Ferri, D., Mondelli, C., Krumeich, F., and Baiker, A.: Discrimination of active palladium sites in catalytic liquid-phase
686 oxidation of benzyl alcohol, *J. Phys. Chem. B.*, 110, 46, 22982-22986, doi:10.1021/jp065779z, 2006.
- 687
- 688 Finewax, Z., de Gow, J. A., and Ziemann, P. J.: Identification and Quantification of 4-Nitrocatechol Formed from OH
689 and NO₃ Radical-Initiated Reactions of Catechol in Air in the Presence of NO_x: Implications for Secondary Organic
690 Aerosol Formation from Biomass Burning, *Environmental Science & Technology*, 52 (4), 1981-1989, doi:
691 10.1021/acs.est.7b05864, 2018.
- 692
- 693 Fu, Zi., Xie, H., Elm, J., Guo, X., Fu, Zh., and Chen, J.: Formation of low-volatile products and unexpected high
694 formaldehyde yield from the atmospheric oxidation of methylsiloxanes, *Environ. Sci. Technol.*, 54, 12, 7136-7145,
695 doi:10.1021/acs.est.0c01090, 2020.
- 696
- 697 Gkatzelis, G. I., Coggon, M. M., McDonald, B. C., Peischl, J., Aikin, K. C., Gilman, J. B., Trainer, M., and Warneke, C.:
698 Identifying volatile chemical product tracer compounds in U.S. Cities, *Environ. Sci. Technol.*,
699 doi:10.1021/acs.est.0c05467, 55, 188–199, 2021.
- 700
- 701 Gowda, D., Kawamura, K., and Tachibana, E.: Identification of hydroxy- and keto-dicarboxylic acids in remote marine
702 aerosols using gas chromatography/quadruple and time-of-flight mass spectrometry, *Rapid Communications in Mass
703 Spectrometry*, 30(7), 992–1000, doi: 10.1002/rcm.7527, 2016.
- 704
- 705 Harrison, J. C., and Wells, J. R.: Gas-phase chemistry of benzyl alcohol: reaction rate constants and products with OH
706 radical and ozone, *Atmos. Environ.*, 43, 798–804, 2009.



707

708 Harrison, J. C., and Wells, J. R.: 2-Butoxyethanol and benzyl alcohol reactions with the nitrate radical: rate coefficients
709 and gas-phase products, *Int. J. Chem. Kinet.*, 44, 778–788, 2012.

710

711 Hayes, P. L., Carlton, A. G., Baker, K. R., Ahmadov, R., Washenfelder, R. A., Alvarez, S., Rappenglück, B., Gilman, J.
712 B., Kuster, W. C., de Gouw, J. A., Zotter, P., Prévôt, A. S. H., Szidat, S., Kleindienst, T. E., Offenberg, J. H., Ma, P. K.,
713 and Jimenez, J. L.: Modeling the formation and aging of secondary organic aerosols in Los Angeles during CalNex 2010,
714 *Atmos. Chem. Phys.*, 15, 5773–5801, 2015.

715

716 Hinton, M. R.: Xylaric acid, D-arabinaric acid (D-lyxaric acid), L-arabinaric acid (L-lyxaric acid), and Ribaric acid-1,4-
717 lactone; Synthesis and isolation-synthesis of polyhydroxypolyamides therefrom, Theses, Dissertations, & Professional
718 Papers. 1202, <https://scholarworks.umt.edu/etd/1202>, 2008.

719

720 Hodzic, A., Jimenez, J. L., Madronich, S., Aiken, A. C., Bessagnet, B., Curci, G., Fast, J., Lamarque, J.-F., Onasch, T.
721 B., Roux, G., Schauer, J. J., Stone, E. A., and Ulbrich, I. M.: Modeling organic aerosols during MILAGRO: importance
722 of biogenic secondary organic aerosols, *Atmos. Chem. Phys.*, 9, 6949–6981, 2009.

723

724 Horvat, R. J., Chapman, G. W., Jr., Robertson, J. A., Meredith, F. I., Scorza, R., Callahan, A. M., and Morgens, P.:
725 Comparison of the volatile compounds from several commercial peach cultivars, *J. Agric. Food Chem.*, 38, 234–237,
726 1990.

727

728 Humes, M. B., Wang, M., Kim, S., Machesky, J. E., Gentner, D. R., Robinson, A. L., Donahue, N. M., and Presto, A. A.:
729 Limited secondary organic aerosol production from acyclic oxygenated volatile chemical products, *Environ. Sci. Technol.*
730 56, 4806–4815, 2022.

731

732 Humpf, H. U., and Schreier, P.: Bound aroma compounds from the fruit and the leaves of blackberry (*Rubus laciniata* L.),
733 *J. Agric. Food Chem.*, 39, 1830–1832, 1991.

734



- 735 Ikemori, E., Nakayama, T., and Hasegawa, H.: Characterization and possible sources of nitrated mono- and di-aromatic
736 hydrocarbons containing hydroxyl and/or carboxyl functional groups in ambient particles in Nagoya, Japan, *Atmos.*
737 *Environ.*, 211, 91-102, 2019.
- 738
- 739 Janecek, N. J., Marek, R. F., Bryngelson, N., Singh, A., Bullard, R. L., Brune, W. H., and Stanier, C. O.: Physical
740 properties of secondary photochemical aerosol from OH oxidation of a cyclic siloxane, *Atmos. Chem. Phys.*, 19, 1649–
741 1664, 2019.
- 742
- 743 Jaoui, M., and Kamens, R. M.: Mass balance of gaseous and particulate products analysis from α -pinene/ NO_x /air in the
744 presence of natural sunlight, *J. Geophys. Res.*, 106, D12, 12,541-12,558, doi:10.1029/2001JD900005, 2001.
- 745
- 746 Jaoui, M., Kleindienst, T. E., Lewandowski, M., and Edney, E. O.: Identification and quantification of aerosol polar
747 oxygenated compounds bearing carboxylic and/or hydroxyl groups, 1. Method development, *Anal. Chem.*, 76, 4765–
748 4778, 2004.
- 749
- 750 Jaoui, M., Kleindienst, T. E., Lewandowski, M., Offenberg, J. H., and Edney, E. O.: Identification and quantification of
751 aerosol polar oxygenated compounds bearing carboxylic or hydroxyl groups. 2. Organic tracer compounds from
752 monoterpenes, *Environ. Sci. Technol.*, 39, 5661–5673, 2005.
- 753
- 754 Jaoui, M., Kleindienst, T. E., Docherty, K. S., Lewandowski, M., and Offenberg, J. H.: Secondary organic aerosol
755 formation from the oxidation of a series of sesquiterpenes: α -cedrene, β -caryophyllene, α -humulene and α -farnesene with
756 O_3 , OH and NO_3 radicals, *Environ. Chem.* 10, 178–193, doi:10.1071/EN13025, 2013.
- 757
- 758 Jaoui, M., Lewandowski, M., Docherty, K., Offenberg, J. H., and Kleindienst, T. E.: Atmospheric oxidation of 1,3-
759 butadiene: characterization of gas and aerosol reaction products and implications for $\text{PM}_{2.5}$, *Atmos. Chem. Phys.*, 13681–
760 13704, doi: 10.5194/acp-14-1368114, 2014.
- 761



762 Jaoui, M., Lewandowski, M., Offenberg, H. J., Colon, M., Docherty, K. S., and Kleindienst, T. E.: Characterization of
763 aerosol nitroaromatic compounds: Validation of an experimental method, *Mass Spectrom.*, 53, 680–692, 2018.
764
765 Jaoui, M., Szmigielski, R., Nestorowicz, K., Kolodziejczyk, A., Sarang, K., Rudzinski, K. J., Konopka, A., Bulska, E,
766 Lewandowski, M., And Kleindienst, T. E.: Organic hydroxy acids as highly oxygenated molecular (HOM) tracers for
767 aged isoprene aerosol, *Environmental Science & Technology*, 53 (24), 14516-14527, doi: 10.1021/acs.est.9b05075, 2019.
768
769 Jaoui, M., Piletic, I., Szmigielski, R., Rudzinski, J. K., E, Lewandowski, M., Riedel, T. P., and Kleindienst, T. E.: Rapid
770 production of highly oxidized molecules in isoprene aerosol via peroxy and alkoxy radical isomerization pathways in low
771 and high NO_x environments: Combined laboratory, computational and field studies, *Science of The Total Environment*,
772 775, 145592, doi: 10.1016/j.scitotenv.2021.145592, 2021
773
774 Jenkin, M. E., Saunders, S. M., Wagner, V., and Pilling, M. J.: Protocol for the development of the Master Chemical
775 Mechanism, MCM v3 (Part B): tropospheric degradation of aromatic volatile organic compounds, *Atmos. Chem. Phys.*,
776 3, 181–193, <https://doi.org/10.5194/acp-3-181-2003>, 2003.
777
778 Khare, P., and Gentner, D. R.: Considering the future of anthropogenic gas-phase organic compound emissions and the
779 increasing influence of non-combustion sources on urban air quality, *Atmos. Chem. Phys.*, 18, 5391–5413, 2018.
780
781 Kleindienst, T. E., Edney, E. O., Lewandowski, M., Offenberg, J. H., and Jaoui M.: Secondary organic carbon and aerosol
782 yields from the irradiations of isoprene and α -pinene in the presence of NO_x and SO₂, *Environ. Sci. Technol.*, 40, 3807–
783 3812, 2006.
784
785 Kleindienst, T. E., Lewandowski, M., Offenberg, J. H., Jaoui, M., and Edney, E. O.: The formation of secondary organic
786 aerosol from the isoprene + OH reaction in the absence of NO_x, *Atmos. Chem. Phys.*, 9, 6541–6558, 2009.
787



- 788 Kleindienst, T. E., Jaoui, M., Lewandowski, M., Offenberg, J. H., and Docherty, K. S.: The formation of SOA and
789 chemical tracer compounds from the photooxidation of naphthalene and its methyl analogs in the presence and absence
790 of nitrogen oxides, *Atmos. Chem. Phys.*, doi:10.5194/acp-12-8711-2012, 12, 8711–8726, 2012.
- 791
- 792 Kroflic, A., Hus, M., Grilc, M., and Grgic, I.: Underappreciated and complex role of nitrous acid in aromatic nitration
793 under mild environmental conditions: the case of activated methoxyphenols, *Environ. Sci. Technol.*, 52, 13756–13765,
794 <https://doi.org/10.1021/acs.est.8b01903>, 2018.
- 795
- 796 Kroll, J. H., Chan, A. W. H., Ng, N. L., Flagan, R. C., and Seinfeld, J. H.: Reactions of semivolatile organics and their
797 effects on secondary organic aerosol formation, *Environ. Sci. Technol.*, 41, 3545–3550, 2007.
- 798
- 799 Larsen, M., and Poll, L.: Odor thresholds of some important aroma compounds in raspberries, *Z. Lebensm. Unters. Forsch.*,
800 191, 129–131, 1990.
- 801
- 802 Lewandowski, M., Jaoui, M., Offenberg, J. H., Krug, J. D., and Kleindienst, T. E.: Atmospheric oxidation of isoprene and
803 1,3-butadiene: influence of aerosol acidity and relative humidity on secondary organic aerosol, *Atmos. Chem. Phys.*, 15,
804 3773–3783, doi:10.5194/acp-15-3773-2015, 2015.
- 805
- 806 Li, W., Li, L., Chen, C-L, Kacarab, M., Peng, W., Price, D., Xu, J., and Cocker III, D. R.: Potential of select intermediate-
807 volatility organic compounds and consumer products for secondary organic aerosol and ozone formation under relevant
808 urban conditions, *Atmos. Environ.*, 118, 109–117, 2018.
- 809
- 810 Lu, Q., Murphy, B. N., Momei Q., Adams, P. J., Zhao, Y., Pye, H. O. T., Efstathiou, C., Allen, C., and Robinson, A. L.:
811 Simulation of organic aerosol formation during the CalNex study: updated mobile emissions and secondary organic
812 aerosol parameterization for intermediate-volatility organic compounds, *Atmos. Chem. Phys.*, 20, 4313–4332, 2020.
- 813
- 814 McDonald, B. C., De Gouw, J. A., Gilman, J. B., Jathar, S. H., Akherati, A., Cappa, C. D., Jimenez, J. L., Lee-Taylor, J.,
815 Hayes, P. L., McKeen, S. A., Cui, Y. Y., Kim, S. W., Gentner, D. R., Isaacman-VanWertz, G., Goldstein, A. H., Harley,



- 816 R. A., Frost, G. J., Roberts, J. M., Ryerson, T. B., and Trainer, M.: Volatile chemical products emerging as largest
817 petrochemical source of urban organic emissions, *Science*, 359, 760–764, 2018.
- 818
- 819 Milani, A., Al-Naiema, I. M., and Stone, E. A.: Detection of a secondary organic aerosol tracer derived from personal care
820 products, *Atmos. Environ.*, 246, 118078, 2021.
- 821
- 822 Mohr, C., DeCarlo, P. F., Heringa, M. F., Chirico, R., Richter, R., Crippa, M., Querol, X., Baltensperger, U., and Prévôt,
823 A. S. H.: Spatial variation of aerosol chemical composition and organic components identified by positive matrix
824 factorization in the Barcelona region, *Environ. Sci. Technol.*, 49, 10421–10430, 2015.
- 825
- 826 Namysl, S., Pelucchi, M., Maffei, L. P., Herbinet, O., Stagni, A., Faravelli, T., and Battin-Leclerc, F.: Experimental and
827 modeling study of benzaldehyde oxidation, *Combustion and Flame*, 211, 124–132, 2020.
- 828
- 829 Offenberg, J. H., Lewandowski, M., Edney, E. O., Kleindienst, T. E., Jaoui, M.: Investigation of a systematic offset in the
830 measurement of organic carbon with a semicontinuous analyzer, *J. A&WMA*, 57:5, 596-599, doi:10.3155/1047-
831 3289.57.5.596, 2007
- 832
- 833 Orlova, I., Marshall-Colón, A., Schnepf, J., Wood, B., Varbanova, M., Fridman, E., Blakeslee, J. J., Peer, W. A., Murphy,
834 A. S., Rhodes, D., Pichersky, E., and Dudareva, N.: Reduction of Benzenoid synthesis in petunia flowers reveals multiple
835 pathways to benzoic acid and enhancement in auxin transport, *Plant Cell*, 18, 3458–3475, 2006.
- 836
- 837 Pennington, E. A., Seltzer, K. M., Murphy, B. N., Qin, M., Seinfeld, J. H., Pye, H. O. T.: Modeling secondary organic
838 aerosol formation from volatile chemical products, *Atmos. Chem. Phys.*, doi:10.5194/acp-21-18247-18261-2021, 18247-
839 18261, 2021.
- 840
- 841 Piletic, I. R., and Kleindienst, T. E.: Rates and Yields of Unimolecular Reactions Producing Highly Oxidized Peroxy
842 Radicals in the OH-Induced Autoxidation of α -Pinene, β -Pinene, and Limonene, *The Journal of Physical Chemistry A*,
843 126 (1), 88-100, doi: 10.1021/acs.jpca.1c07961, 2022.



844

845 Qin, M. M., Murphy, B. N., Isaacs, K. K., McDonald, B. C., Lu, Q. Y., McKeen, S. A., Koval, L., Robinson, A. L.,
846 Efstathiou, C., Allen, C., and Pye, H. O. T.: Criteria pollutant impacts of volatile chemical products informed by near-
847 field modelling, *Nature Sustainability*, 4, 129–137, <https://doi.org/10.1038/s41893-020-00614-1>, 2021.

848

849 Rohl, A., and Lammedl. G.: Determination of malic acid and other C4 dicarboxylic acids in atmospheric aerosol samples,
850 *Chemosphere*, 46(8), 1195-1199, doi: 10.1016/s0045-6535(01)00243-0, 2002.

851

852 Sankar, S., Nowicka, E., Carter, E., Murphy, D. M., Knight, D. W., Bethell, D., and Hutchings, G. J.: The benzaldehyde
853 oxidation paradox explained by the interception of peroxy radical by benzyl alcohol, *Nature Communic*,
854 doi:10.1038/ncomms4332, 5, 3332, 2014.

855

856 Seltzer, K. M., Murphy, B. N., Pennington, E. A., Allen, C., Talgo, K., and Pye, H. O. T.: Volatile chemical product
857 enhancements to criteria pollutants in the United States, *Environ. Sci. technol.*, doi:10.1021/acs.est.1c04298, 2021.

858

859 Shilling, J. E., Chen, Q., King, S. M., Rosenoern, T., Kroll, J. H., Worsnop, D. R., McKinney, K. A., and Martin, S. T.:
860 Particle mass yield in secondary organic aerosol formed by the dark ozonolysis of α -pinene, *Atmos. Chem. Phys.*, 8,
861 2073–2088, doi:10.5194/acp-8-2073-2008, 2008.

862

863 Smith, D. F., Kleindienst, T. E., and Hudgens, E. E.: Improved high-performance liquid chromatographic method for
864 artifact free measurements of aldehydes in the presence of ozone using 2,4-dinitrophenylhydrazine, *J. Chromatogr. A*,
865 483, 431–436, 1989.

866

867 Stockwell, C. E., Coggon, M. M., Gkatzelis, G. A., Ortega, J., McDonald, B. C., Peischl, J., Aikin, K., Gilman, J. B.,
868 Trainer, M., and Warneke, C.: Volatile organic compound emissions from solvent- and water borne coatings:
869 compositional differences and tracer compound identifications, *Atmos. Chem. Phys.*, 21, 6005–6022, doi:10.5194/acp-
870 21-6005-2021, 2021.

871



- 872 Urakami, K., Kobayashi, C., Miyazaki, Y., Nishijima, K., and Yoshimura, Y.: Degradation products generated by
873 sonication of benzyl alcohol, a sample preparation solvent for the determination of residual solvents in pharmaceutical
874 bulks, on capillary gas chromatography, *Chem. Pharm. Bull.*, 48, 1299–1303, 2000.
- 875
- 876 Vallat, A., and Dorn, S.: Changes in volatile emissions from apple trees and associated response of adult female codling
877 moths over the fruit-growing season, *J. Agric. Food Chem.*, 53, 4083–4090, 2005.
- 878
- 879 Vidovic, K., Lasic Jurkovic, D., Sala, M., Kroflic, A., and Grgic, I.: Nighttime aqueous-phase formation of nitrocatechols
880 in the atmospheric condensed phase, *Environ. Sci. Technol.*, 52, 9722– 9730, <https://doi.org/10.1021/acs.est.8b01161>,
881 2018.
- 882
- 883 Vlachou, A., Daellenbach, K. R., Bozzetti, C., Chazeau, B., Salazar, G. A., Szidat, S., Jaffrezo, J. L., Hueglin, C.,
884 Baltensperger, U., El Haddad, I., and Prévôt, A. S.: Advanced source apportionment of carbonaceous aerosols by coupling
885 offline AMS and radiocarbon size-segregated measurements over a nearly 2-year period. *Atmos. Chem. Phys.*, 18, 6187–
886 6206, 2018.
- 887
- 888 Wang, L.: The atmospheric oxidation mechanism of benzyl alcohol initiated by OH radicals: the addition channels, *Chem.*
889 *Phys. Chem.*, 16 (7), 1542-1550, doi:10.1002/cphc.201500012, 2015.
- 890
- 891 Wang, N., Jorga, S. D., Pierce, J. R., Donahue, N. M., and Pandis, S. N.: Particle wall-loss correction methods in smog
892 chamber experiments, *Atmos. Meas. Tech.*, 11, 6577–6588, doi:10.5194/amt-11-6577-2018, 2018.
- 893
- 894 Wang, Y., Hu, M., Wang, Y., Zheng, J., Shang, D., Yang, Y., Liu, Y., Li, X., Tang, R., Zhu, W., Du, Z., Wu, Y., Guo, S.,
895 Wu, Z., Lou, S., Hallquist, M., and Yu, J. Z.: The formation of nitro-aromatic compounds under high NO_x and
896 anthropogenic VOC conditions in urban Beijing, China, *Atmos. Chem. Phys.*, 19, 7649–7665, 2019.
- 897
- 898 Weschler, C. J.: Chemistry in indoor environments: 20 years of research, *Indoor Air*, 21 (3), 205-218, 2011.
- 899



900 Wu, Y., and Johnston, M. V.: Molecular characterization of secondary aerosol from oxidation of cyclic methylsiloxanes,
901 J. Am. Soc. Mass. Spectr., 27, 402–409, doi:10.1007/s13361-015-1300-1, 2016.

902

903 Wu, Y., and Johnston, M. V.: Aerosol formation from OH oxidation of the volatile cyclic methyl siloxane (cVMS)
904 Decamethylcyclopentasiloxane, Environ. Sci. Technol., 51, 4445–4451, doi:10.1021/acs.est.7b00655, 2017.

905

906 Zhao, B., Wang, S., Donahue, N. M., Jathar, S. H., Huang, X., Wu, W., Hao, J., and Robinson, A. L.: Quantifying the
907 effect of organic aerosol aging and intermediate volatility emissions on regional-scale aerosol pollution in China, Sci.
908 Rep., 6, 28815, doi:10.1038/srep28815, 2016.

909

910 Zhang, X., Cappa, C. D., Jathar, S. H., McVay, R. C., Ensberg, J. J., Kleeman, M. J., and Seinfeld, J. H.: Influence of
911 vapor wall loss in laboratory chambers on yields of secondary organic aerosol, PNAS, doi:10.1073/pnas.1404727111,
912 111 (16), 5802-5807, 2014.

913

914

915

916

917

918

919

920

921

922

923

924

925

926

927



928 **Table 1.** Initial conditions for BnOH experiments in the presence and absence of NO.

Exp. IDs	BnOH (ppb)	H ₂ O ₂ (ppm)	NO ^a (ppb)	Seed surface area (nm ² cm ⁻³)	BnOH/NO (ppb/ppb)	T (°C)	RH (%)
ER-889	385	-	178	4.67 × 10 ⁷	2.2	24.5	31.0
ER-890	355	-	96	4.94 × 10 ⁷	3.7	24.5	31.1
ER-891	723	-	188	9.88 × 10 ⁷	3.8	24.6	31.3
ER-892	319	3.04	-	1.36 × 10 ⁶	-	25.7	< 4.0

929 T: temperature; RH: relative humidity. Seed aerosol at 1 μg m⁻³. ^a: The initial NO_x during the irradiations was greater than 98% NO.

930

931 **Table 2.** Steady-state GP and reacted BnOH and NO concentration during the irradiations.

Exp. IDs	NO (ppb)	Reacted NO (ppb)	BnOH (ppb)	Reacted BnOH (ppb)	BnOH/NO ratio (ppb/ppb)	O ₃ (ppb)	NO _y (ppb)
ER889	78	100	132	253	1.7	30	163
ER890	9	87	132	223	14.7	147	80
ER891	29	159	387	336	13.4	11	146
ER892	-	-	85	234	-	28	-

932

933 **Table 3.** Formation and yields of SOA (Y_{SOA}) and SOC (Y_{SOC}). All organic and carbon aerosol masses are corrected for
934 a wall loss of 0.067 h⁻¹ (Kleindienst et al., 2012).

Exp. IDs	SOA (μg/m ³)	SOC (μgC/m ³)	SOA/SOC	Y _{SOA} (%)	Y _{SOC} (%)
ER889	39.6	23.2	1.7	3.6	2.7
ER890	56.1	30.3	1.9	5.7	4.0
ER891	119.5	58.9	2.0	8.1	5.1
ER892	52.9	24.8	2.1	5.2	3.1

935

936

937

938

939

940

941

942

943

944

945



946 **Table 4.** Steady state carbonyl concentrations (ppmV) during BnOH oxidation (FH: formaldehyde; AH: acetaldehyde;
947 Ac: acetone; MA: methacrolein; BN: 2-butanone; BnAld: benzaldehyde; G: glyoxal; MG: methylglyoxal).

Exp. ID	FH	AH	Ac	MA	BN	BnAld	G	MG
ER889	2.4	1.2	1.0	1.0	0.6	23.09	5.0	0.6
ER890	1.5	2.8	-	-	2.9	18.2	3.8	0.4
ER891	5.1	2.5	1.3	2.0	1.4	30.8	8.6	0.6
ER892	181.7	23.5	-	0.8	0.8	5.2	7.8	1.6

948

949

950

951

952

953

954

955

956

957

958

959

960

961

962

963

964

965

966

967

968

969



970 **Table 5.** Summary of selected reaction products detected and identified either in gas-phase (GP), particle phase (PP) or
 971 both from BnOH/NO_x, and BnOH/H₂O₂ experiments. Tables 6 and 7 shows additional aerosol species with high oxygen
 972 to carbon ratio and/or nitro group. NA: not applicable. ^a: underivatized m/z are given. *: identified with authentic standard.

IUPAC/common nomenclature	Formula	m/z BSTFA (EI)	MW [MW _{BSTFA}] (g mol ⁻¹)	Proposed Structure	Detected
Benzyl alcohol (BnOH)	C ₇ H ₈ O	165, 91, 135, 180, 73	108 [180]		GP
Phenol	C ₆ H ₆ O	73, 151, 166, 94, 65	94 (166)		GP, PP
Benzaldehyde (BnAld)	C ₇ H ₆ O	106, 105, 77, 77, 51	106 (NA)		GP, PP
Benzene-1,2-diol (catechol)	C ₆ H ₆ O ₂	239, 255, 80, 283, 73	110 (254)		PP
Benzoic acid	C ₇ H ₆ O ₂	179, 105, 135, 77, 194	122 (194)		GP, PP
Salicylaldehyde	C ₇ H ₆ O ₂	179, 105, 135, 77, 194	122 (194)		GP
3-Hydroxy benzaldehyde	C ₇ H ₆ O ₂	179, 105, 135, 77, 194	122 (194)		GP
2-Hydroxybenzyl alcohol (salicyl alcohol)	C ₇ H ₈ O ₂	73, 253, 179, 268, 147	124 (268)		GP, PP
4-Hydroxybenzyl alcohol	C ₇ H ₈ O ₂	73, 179, 253, 268, 147	124 (268)		GP, PP
4-Hydroxybenzoic acid (<i>p</i> -salicylic acid)	C ₇ H ₆ O ₃	267, 223, 193, 282, 73	138 (282)		PP [H ₂ O ₂]

973



974 **Table 6.** Highly oxygenated products ($O:C > 1.3$) identified in benzyl alcohol photooxidation in the presence of NO_x , or
 975 H_2O_2 . *: identified with authentic standard. *L*-Tartaric acid and *D*-tartaric acid co-elute. The structure of 4-oxo-*D*-arabonic
 976 acid isomer and 2,3,5-Trihydroxy-4-oxopentanal isomer are shown for trihydroxy-oxo-pentanoic acid, and trihydroxy-oxo-
 977 oxo-pentanal, respectively. Four peaks with similar fragments/adducts as pentaric acid were observed.

Nomenclature	Chemical Formulae	O/C Ratio (by wt)	m/z BSTFA Derivative (CI-CH ₄); (EI)	MW (MW _{BSTFA})	Proposed Structure
Epoxy succinic acid (2 peaks)	C ₄ H ₄ O ₅	1.7	187, 261, 73, 277, 173 73, 173, 261, 129, 143	132 (276)	
2-Hydroxybutanedioic acid* (malic acid)	C ₄ H ₆ O ₅	1.7	233, 335, 73, 307, 351 73, 147, 233, 245, 335	134 (350)	
Trihydroxy-oxo-pentanal (5 peaks)	C ₅ H ₈ O ₅	1.3	73, 275, 203, 349, 393 147, 73, 349, 233, 259	148 (364)	
meso-Tartaric acid*	C ₄ H ₆ O ₆	2.0	423, 321, 277, 439, 73 73, 147, 292, 219, 423	150 (438)	
L-Tartaric acid*	C ₄ H ₆ O ₆	2.0	423, 321, 277, 439, 73 73, 147, 292, 219, 423	150 (438)	
Trihydroxy-oxo-pentanoic acid (8 peaks)	C ₅ H ₈ O ₆	1.6	73, 437, 363, 481, 493 217, 73, 147, 437, 292	164 (452)	
D-Arabinonic acid* (Arabic acid)	C ₅ H ₁₀ O ₆	1.6	361, 217, 73, 435, 525 204, 437, 73, 147, 319	166 (526)	
Pentaric acid* (4 peaks)	C ₅ H ₈ O ₇	1.9	525, 333, 407, 435, 73 73, 292, 189, 407, 525	180 (540)	

978

979

980

981



982 **Table 7.** NACs identified in benzyl alcohol photooxidation in the presence of NO_x.

Nomenclature	Chemical Formula Rt (min)	<i>m/z</i> BSTFA Derivative (CH ₄ -CI) (EI)	MW (MW _{bstfa})	Observed in GP; PP [GP/PP ratio]	Proposed Structure
3-nitrobenzyl alcohol ^a	C ₇ H ₇ NO ₃ (25.93)	226, 210, 180, 136, 73 210, 180, 165, 194, 73	153 (225)	PP, GP [1.71]	
4-nitrocatechol ^a	C ₆ H ₅ NO ₄ (30.86)	300, 284, 328, 254, 73 73, 284, 299, 269, 223	155 (299)	PP, GP [0.08]	
2-hydroxy-5-nitrobenzyl alcohol ^a (4 isomers)	C ₇ H ₇ NO ₄ (34.26)	314, 298, 268, 342, 73 298, 283, 191, 314, 73	169 (313)	PP, GP [0.08]	
2-nitro phloroglucinol ^a (4 isomers) ^b	C ₆ H ₅ NO ₅ (35.62)	388, 372, 416, 428, 73 73, 372, 387, 284, 306	171 (387)	PP	
3,4-dihydroxy-5-nitrobenzyl alcohol (4 isomers) ^c	C ₇ H ₇ NO ₅ (38.18)	388, 372, 416, 428, 73 73, 224, 3876, 401, 356	185 (401)	PP	

983 ^a: identified using authentic standards. ^b: Three additional peaks eluted at 33.76, 34.70, 34.76 min with similar mass spectra
 984 as those recorded for 2-nitro phloroglucinol standard were detected, and the structure given here is for 2-
 985 nitro phloroglucinol. ^c: Three additional peaks eluted at 35.94, 36.60, 38.18 min with similar mass spectra were detected.

986

987

988

989

990

991

992

993

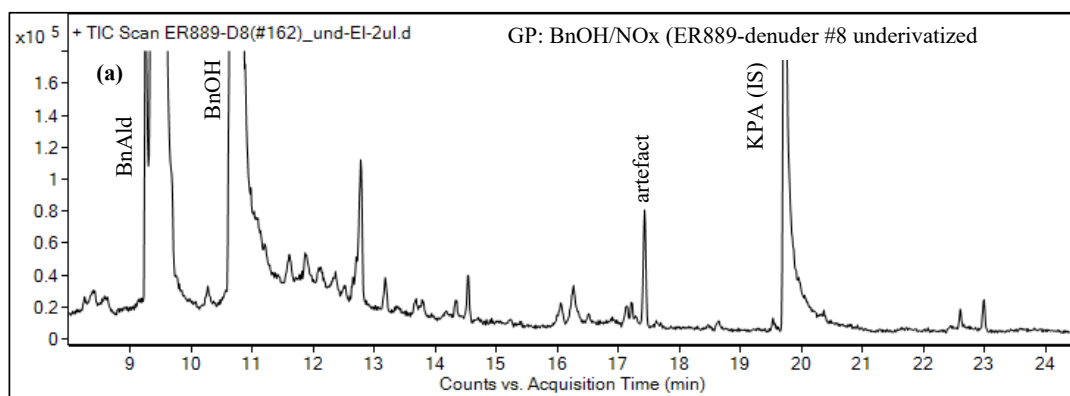
994

995

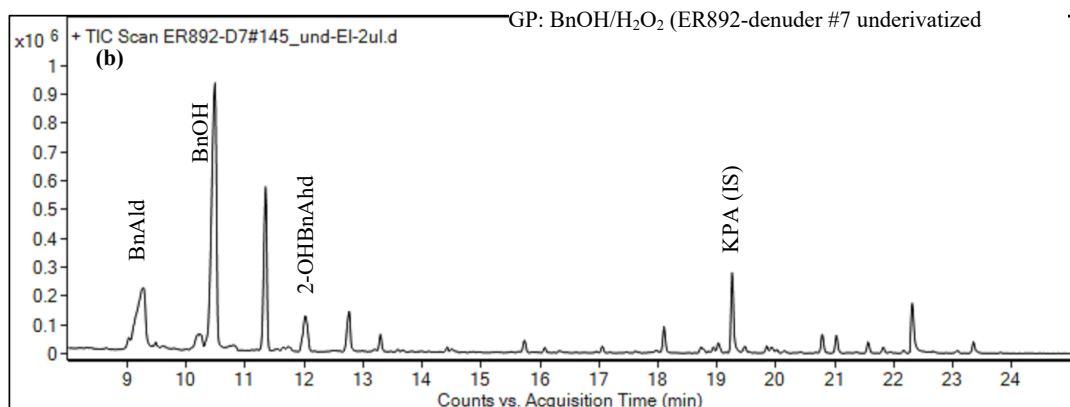
996



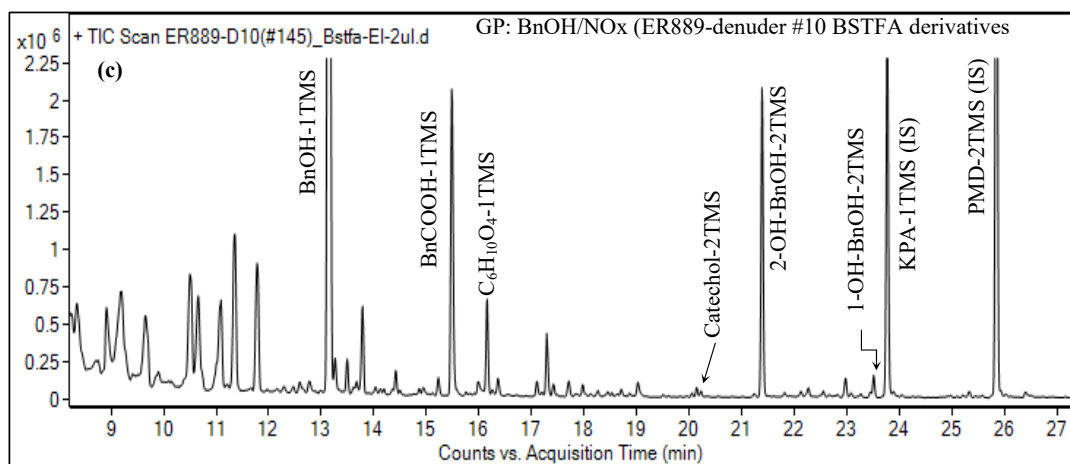
997



998



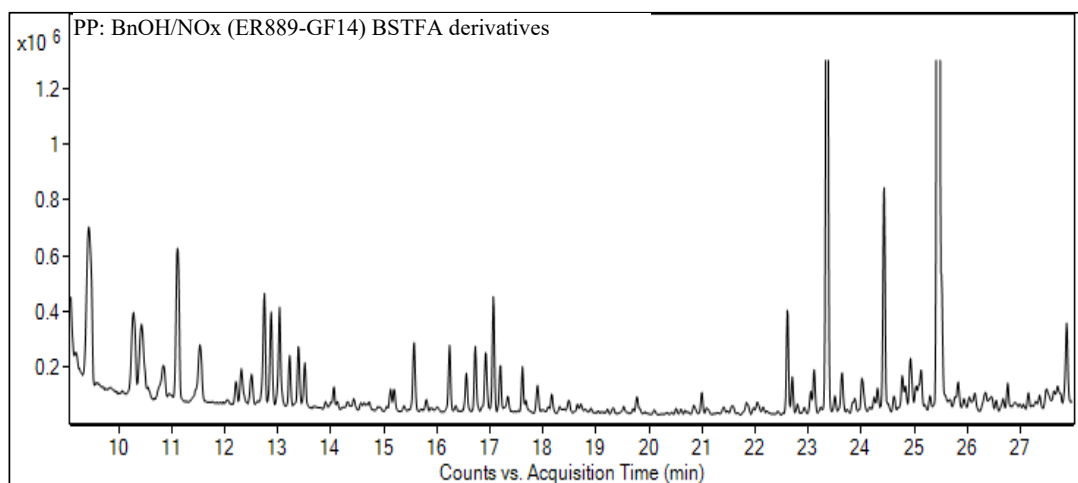
999



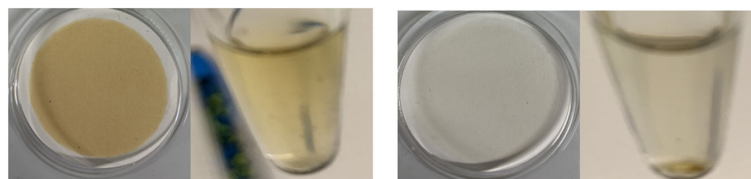
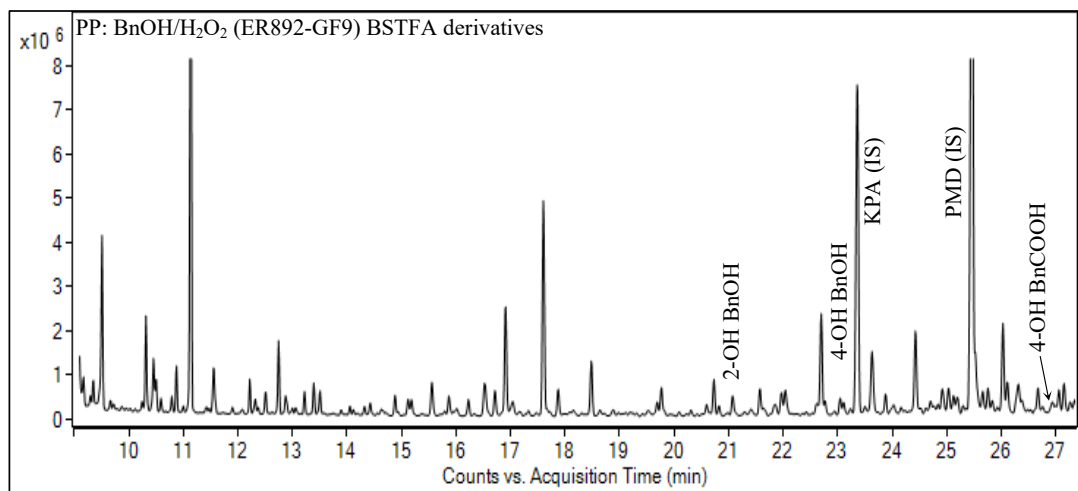
1000 **Figure 1.** Portion of GC-MS total ion chromatogram in EI mode of GP underivatized denuder extract (a) ER-889 (presence of NOx),
1001 (b) ER-892 (absence of NOx), and (c) ER889- (presence of Nox) as BSTFA derivatives.



1002



1003



1004

F1: BnOH/NOx E1: methanol extract F2: BnOH/H2O2 E2: methanol extract

1005

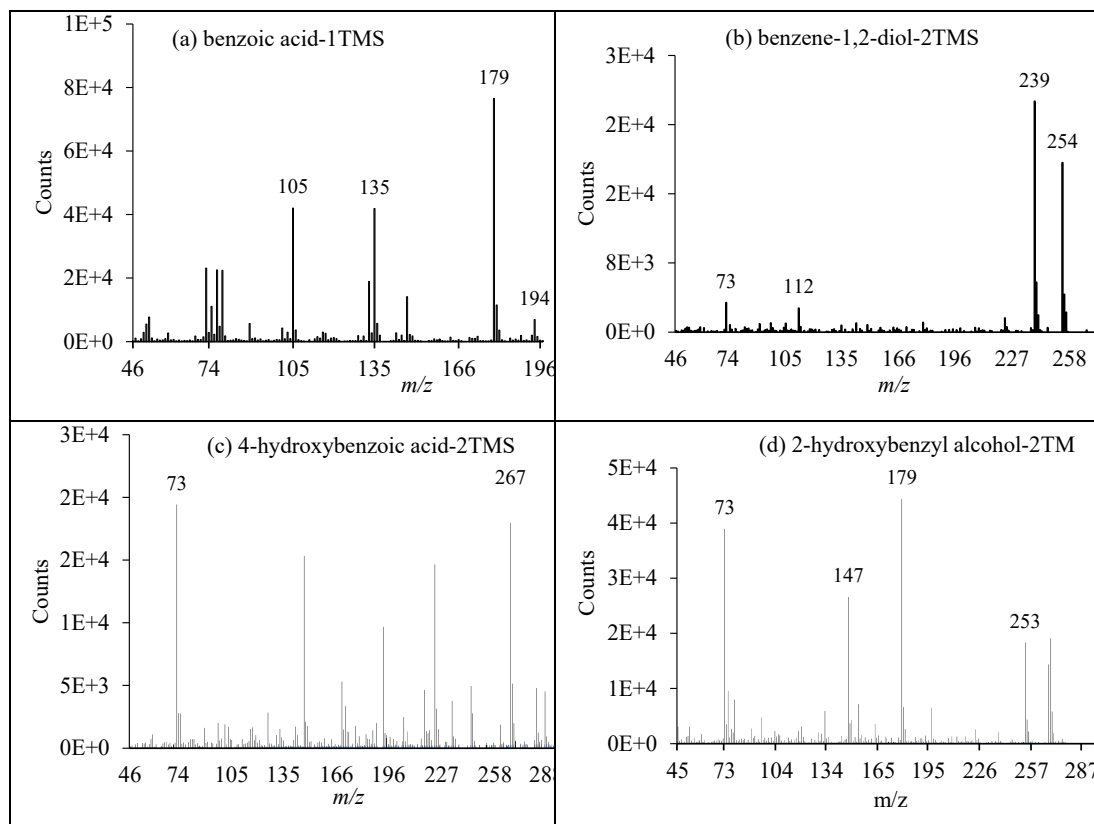
Figure 2. Portion of GC-MS total ion chromatograms (EI mode) of particle-phase extracts: (top) BSTFA derivatized sample form ER-

1006

889 (presence of NOx), (middle) BSTFA derivatives from ER-892 (absence of NOx), (bottom) effect of mixture changes in filter and

1007

methanol extract appearance: BnOH/NOx filter (F1); BnOH/H₂O₂ (F2). The same volume of air was sampled on each filter.

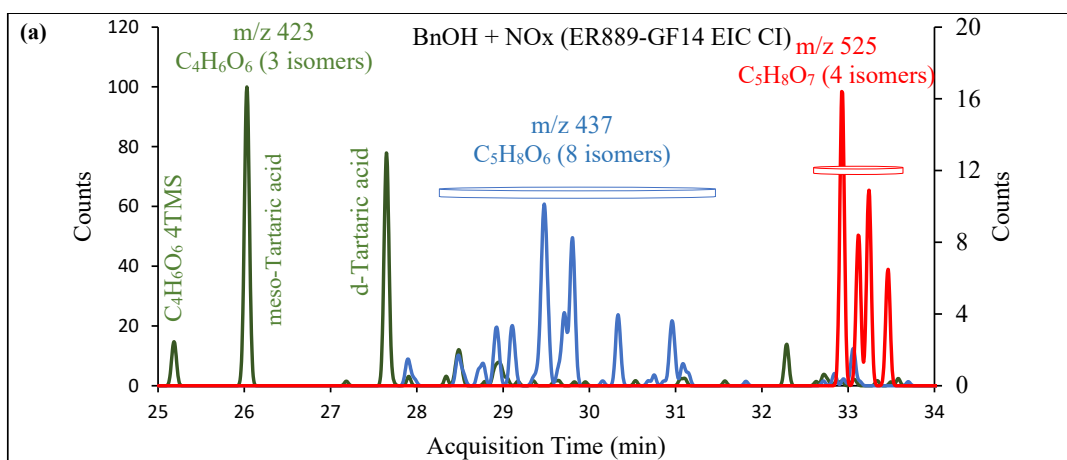


1008 **Figure 3.** Positive EI mass spectra of BSTFA derivatives of selected ring-containing products: benzoic acid, benzene-1,2-diol, 4-
1009 hydroxybenzoic acid; and 2-hydroxybenzyl alcohol.

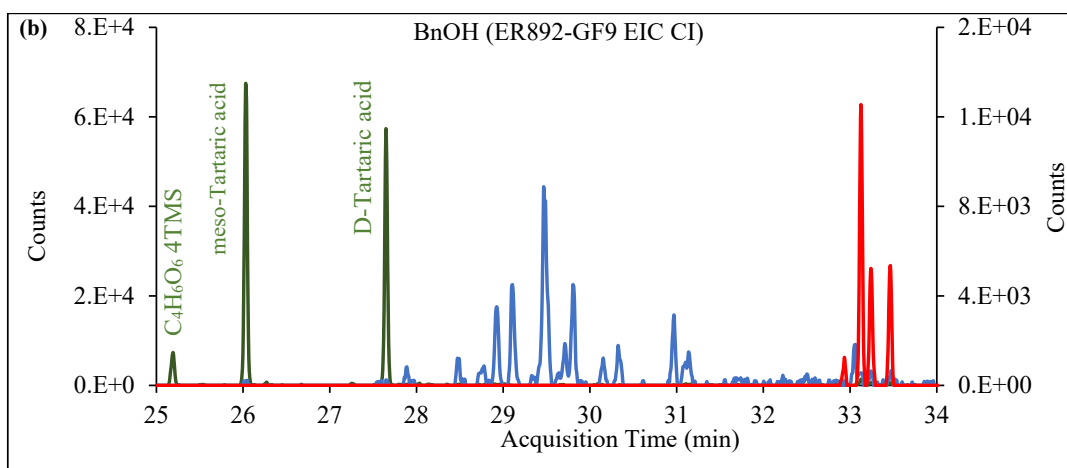
1010
1011
1012
1013
1014



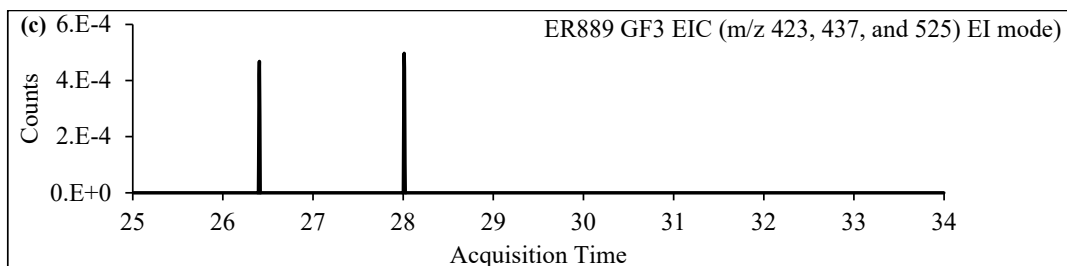
1015



1016



1017

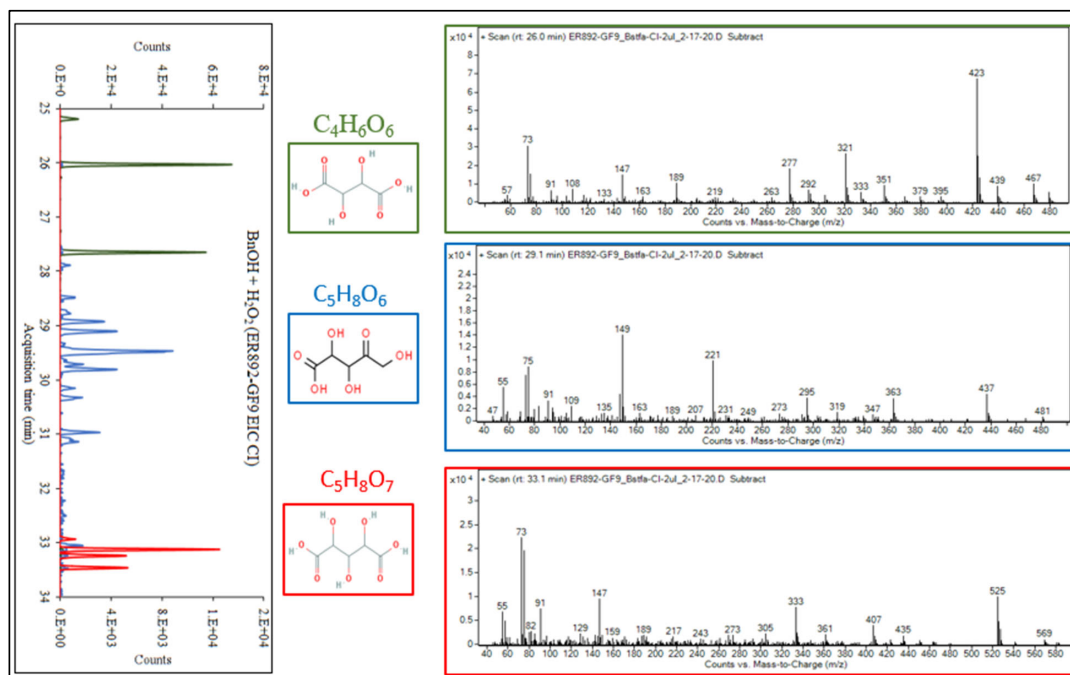


1018

1019

1020

Figure 4. Portion (25–34 min) of GC-MS extracted ion chromatograms (CI-CH₄) at *m/z* 423 (green); *m/z* 437 (blue); and *m/z* 525 (red) merged in one chromatogram (a) BnOH in the presence of NO_x; (b) BnOH in the presence of H₂O₂ and absence of NO_x; (c) Chamber background. Red and top blue: right axis.

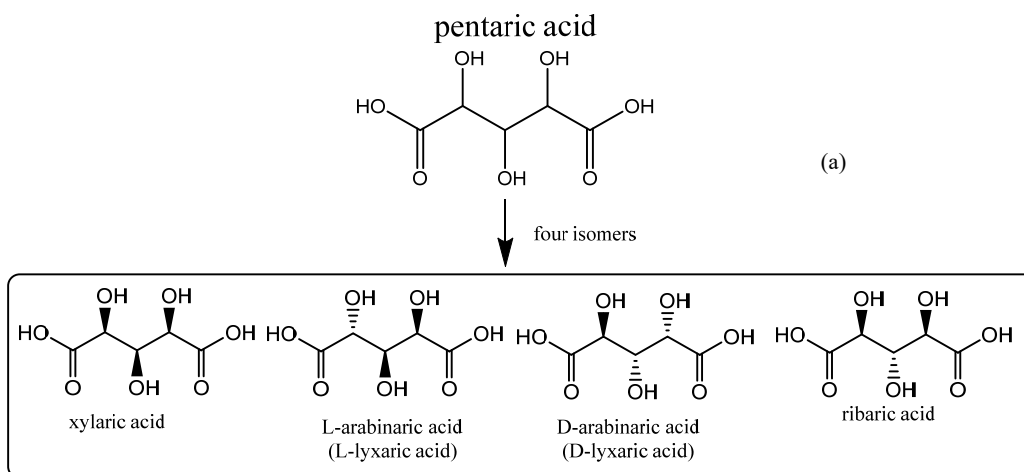


1021
1022
1023
1024
1025
1026
1027
1028
1029
1030
1031
1032

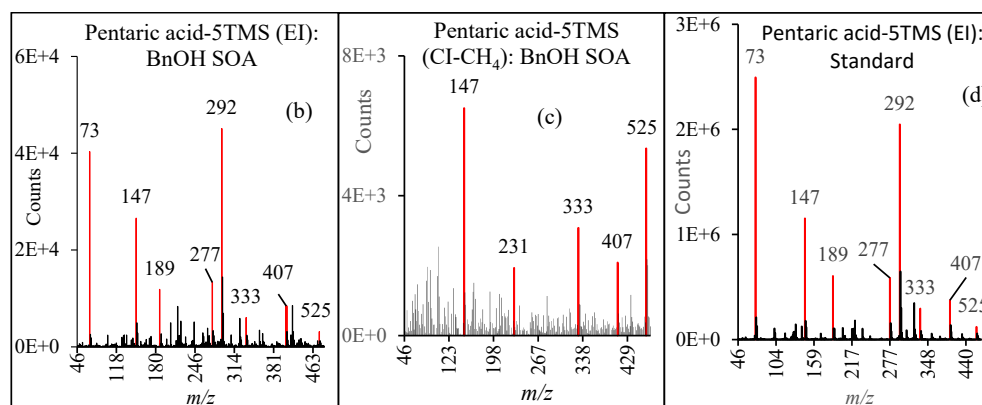
Figure 5. Mass spectra (methane-Cl) of ester TMS derivatives of meso-tartaric acid (top right), trihydroxy-oxo-pentanoic acid (middle right), (c) pentaric acid (bottom right), along with the portion of GC-MS extracted ion chromatograms shown in figure 6. Chemical formulae and chemical structure associated with each group is given in the middle column.



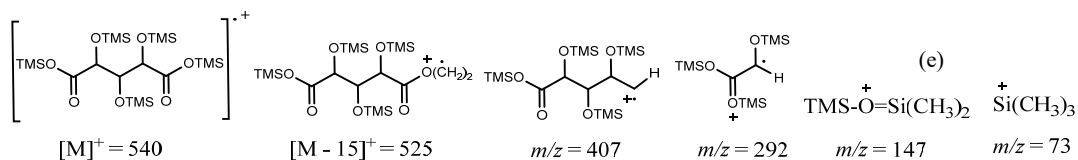
1033



1034



1035



1036

Figure 6. Molecular structures of pentaric acid and its isomers (a); mass spectra of TMS derivatives of pentaric acid acquired for smog chamber SOA (EI: b, CI: c) and authentic standard (d: EI); Major pentaric acid fragments observed in EI mode (e).

1037

1038

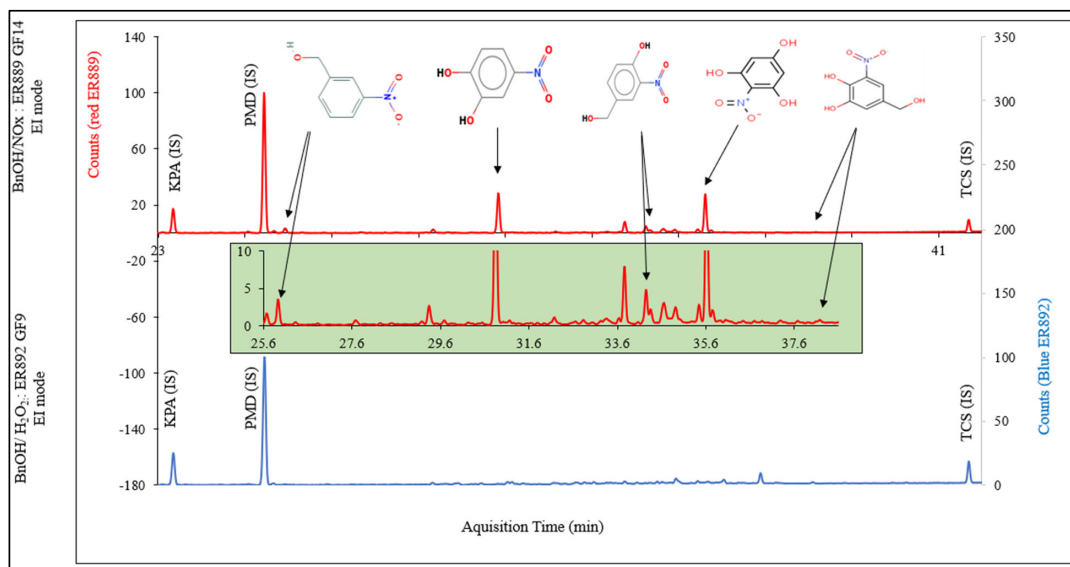
1039

1040

1041

1042

1043



1044

1045 **Figure 7.** Portion of GC-MS extracted ion chromatograms (EI mode) at m/z 210, 165 (IS), 299 (IS), 300, 298, 372, 388 associated with
1046 nitroaromatic compounds merged in one chromatogram (red) BnOH in the presence of NO_x (ER889); (blue) BnOH in the presence of
1047 H₂O₂ and absence of NO_x (ER892).

1048

1049

1050

1051

1052